Heavy-Tailed Class Imbalance and Why Adam Outperforms Gradient Descent on Language Models

Frederik Kunstner[1]
kunstner@cs.ubc.ca

Robin Yadav[1]
robiny12@student.ubc.ca

Alan Milligan[1]
alanmil@cs.ubc.ca

Mark Schmidt[1,2]
schmidtm@cs.ubc.ca

Alberto Bietti[3]
abietti@flatironinstitute.org

[1] University of British Columbia [2] Canada CIFAR AI Chair [3] Flatiron Institute

Abstract

Adam outperforms gradient descent on language models by a larger margin than on other tasks, but it is unclear why. We show that a key factor in this performance gap is the heavy-tailed class imbalance found in language tasks. When trained with gradient descent, the loss of infrequent words decreases more slowly than that of frequent ones, leading to a slow decrease on the average loss as most samples come from infrequent words. Adam and sign-like methods are less sensitive to this problem. To establish that this behavior is caused by class imbalance, we reproduced it across architectures and data types, on language transformers, vision CNNs, and linear models. On a linear model with cross-entropy loss, we show that class imbalance leads to imbalanced, correlated gradients and Hessians that have been hypothesized to benefit Adam, and prove that, in continuous time, gradient descent converges slowly on low-frequency classes while sign descent does not.

1 Introduction

The recent success of large language models such as GPT-3 (Brown et al., 2020) and its successors has relied on costly training procedures at unprecedented scale. A key ingredient in their training is the Adam optimizer (Kingma and Ba, 2015), which outperforms stochastic gradient descent (SGD) by a large margin. Despite this large performance gap, we have a poor understanding of why Adam works better and it has been difficult to find new optimizers that consistently improve over it (Schmidt et al., 2021), especially as we do not know what "problem" Adam solves to outperform SGD.

The success of Adam on language tasks is well documented. Multiple works have found metrics that correlate with its improved performance, showing that it yields uniform updates (Liu et al., 2020), more local progress (Pan and Li, 2023), and that a variant of the condition number is smaller over its path (Jiang et al., 2022). But these observations do not provide a mechanism explaining what property of the problem leads to the improved performance of Adam. Plausible mechanisms have been put forward, but do not provide a complete explanation. Zhang et al. (2020b) show that Adam-like methods are more resilient to heavy-tailed noise, more prominent in language tasks, but noise is not the cause of the gap as it already appears in deterministic training (Kunstner et al., 2023). An alternative hypothesis is that the magnitude of the gradient and Hessian are correlated, justifying clipping (Zhang et al., 2020a). But to justify Adam-like methods, the gradient and Hessian need to be correlated across parameters (Crawshaw et al., 2022). While there is evidence of this correlation in neural networks, we do not know why it would be more pronounced on language rather than vision.

1.1 Contributions

Our goal is to answer *what "problem" makes SGD slow on language tasks but is "fixed" by Adam?*

We argue the problem is what we call heavy-tailed class imbalance, where rare classes account for a large fraction of the data. Language data is imbalanced as some words are much more frequent than

Mathematics of Modern Machine Learning Workshop at NeurIPS 2024.

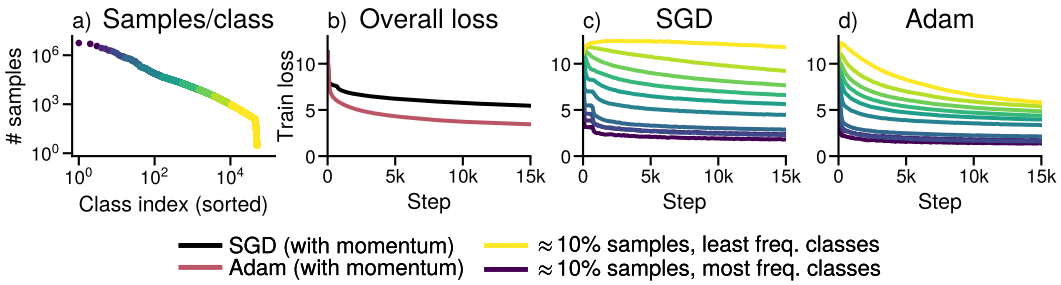

Figure 1: **Gradient descent does not make progress on low-frequency classes, while Adam does.** Training GPT2-Small on WikiText-103. **(a)** Distribution of the classes sorted by class frequency, split into groups corresponding to $\approx 10\%$ of the data. **(b)** Overall training loss. **(c, d)** Training loss for each group using SGD and Adam. SGD makes little to no progress on low-frequency classes while Adam makes progress on all groups. **(b)** is the average of **(c, d)** for the respective optimizer.

others, typically following a power-law. A common modeling assumption is Zipf's law, where the kth most frequent word has frequency $\propto 1/k$ (Piantadosi, 2014). For language tasks framed as next-token prediction, this property is reflected in the tokens and leads to heavy-tailed class imbalance. This contrasts with typical vision datasets such as MNIST, CIFAR, and ImageNet, which are curated to have uniform classes, but also with imbalanced problems with a small number of classes. For example, in binary classification, extreme imbalance implies the minority class has a limited impact on the loss; with an imbalance of 99:1, only 1% of the data comes from the minority class.

The performance gap arises because SGD makes slow progress on rare classes, see Figure 1. On a binary problem, slow performance on 1% of the data need not have a large impact on the average loss if we make fast progress on the remaining 99% of the samples. In contrast, the heavy-tailed class imbalance found in language tasks makes it possible for low-frequency classes to account for most of the data and significantly contribute to the loss, leading to slow performance overall.

We show that heavy-tailed class imbalance makes SGD slow across tasks in Section 2. We show that modifying vision datasets to exhibit heavy-tailed imbalance leads to slow progress with SGD on architectures where the performance gap with Adam is typically smaller. The impact of heavy-tailed imbalance can even be seen on linear models. Additionally, the performance of SGD improves with techniques that address imbalance such as upweighting rare classes.

Our findings provide a simple model where Adam outperforms SGD, a softmax linear model under heavy-tailed class imbalance, which we analyze in Section 3. We show empirically that a correlation between the magnitude of the gradient and Hessian across coordinates, used to justify the benefits of Adam, appears naturally even on a linear model with class imbalance. We provide intuition as to how this pattern emerges through an assignment mechanism that leads to a correlation between class frequencies and the magnitude of the gradient and Hessian across parameters. We additionally prove that, on a simple dataset and in continuous time, GD is slow on low-frequency classes while sign descent is insensitive to the class frequencies.

We do not claim that class imbalance is the only reason Adam outperforms SGD, as other properties of the data or architectures likely also contribute to this gap. Instead, we show that Adam consistently outperforms SGD under heavy-tailed class imbalance. The difficulty of minimizing the loss of minority classes has been explored for binary problems or problems few classes (Anand et al., 1993; Francazi et al., 2023), but the recent scaling of large language models to predictions over more than 100 000 classes puts the problem on a new scale. Our findings indicate that heavy-tailed class imbalance has a significant impact on training performance and should be a consideration for future optimizers to perform well on language and other tasks exhibiting heavy-tailed class imbalance.

2 Experimental results and ablation studies

Figure 1 suggests a correlation between class frequencies and optimization performance that impacts SGD more than Adam. The goal of this section is to verify that (i) class imbalance is a root cause for the performance gap between SGD and Adam, and (ii) whether this gap can be reproduced with simpler algorithms, such as deterministic optimizers, or using sign descent as a proxy for Adam.

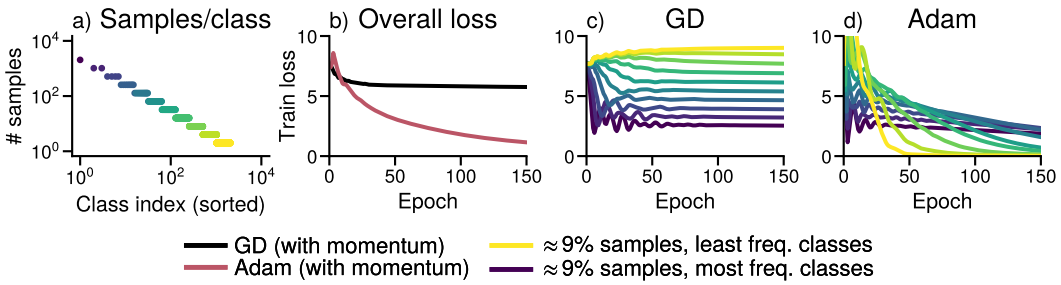

Figure 2: **The impact of heavy-tailed class imbalance is reproducible with linear models.** Softmax regression on synthetic data. The inputs are drawn from a uniform distribution on $[0, 1]^d$. The target classes are heavy-tailed **(a)** and independent of the inputs, but the model can still fit the data as it is overparameterized. **(b, c, d)** Overall training loss and performance of GD and Adam on each subset.

To test these hypotheses, our experiments focus on the training loss as our objective is to understand what makes optimization difficult. We use a constant step-size tuned by grid search. For visualization, we split the data into groups of classes with similar frequencies, as in Figure 1. E.g., for 10 groups, the first group corresponds to $\approx 10\%$ of the data from the most frequent classes. This grouping is only used for visualization and does not affect training. The models, datasets and training procedures are detailled in Appendix A. To show that stochasticity is not necessary to reproduce this behavior, we use deterministic updates (i.e., GD instead of SGD) on smaller models in the next sections.

2.1 Reproducing the frequency gap with vision models

Language models are often contrasted with vision models, which do no exhibit a large performance gap between SGD and Adam. To show that the key difference between these settings is the heavy-tailed class imbalance in language data, we replicate this performance gap by making heavy-tailed vision datasets. Appendix B shows results on CNNs, ResNets and vision transformers on imbalanced variants of ImageNet, made imbalanced by subsampling, and MNIST, augmented to feature 10k classes. In all cases, SGD and Adam perform similarly on balanced data, but exhibit a performance gap similar to Figure 1 on imbalanced data.

2.2 Reproducing the frequency gap with a linear model on uniform data

To show that heavy-tailed imbalance alone can lead to the observed difficulties, we reproduce this behavior on a simple setting: a softmax linear model with cross-entropy loss. We create a dataset with class frequencies $\pi_k \propto 1/k$ and draw n samples uniformly from $[0, 1]$ in d dimensions, independently of the label. While there is no relationship to learn, a linear model can separate the data if $n \ll d$ and the optimization problem is still. As on the transformer of Figure 1, GD makes less progress on low-frequency classes than Adam, as shown in Figure 2. This examples illustrates that a problem that might look innocuous at first is hard to optimize with GD due to heavy-tailed imbalance, while the performance of Adam is less impacted. We give more details on the linear model in Appendix C.

2.3 Interactions between optimizer and imbalance

We have shown that heavy-tailed class imbalance leads to different performance across classes, but which part of the training process leads to this behavior remains unclear. We experiment with simple algorithms to answer the following questions. (i) Is the impact of class imbalance due to stochasticity, or does it happen with deterministic training? (ii) Which component of Adam leads to an improved performance? and (iii) If imbalance is the problem, can we improve performance by reweighting?

Class imbalance already impacts deterministic optimization. A natural hypothesis to explain the impact of class imbalance is that rare classes are sampled less often and thus learned more slowly. On the other hand, stochasticity has been found to have little impact on the gap between SGD and Adam (Kunstner et al., 2023). Our confirm that stochasticity is not the root cause of this problem, as experiments in Figure 2 and Appendix B, as well as further examples on small language models trained with GD in Appendix D, reproduce the dynamics of Figure 1 with full batch GD and Adam.

Adam and sign descent perform well under imbalance. Following Kunstner et al. (2023), we check whether the benefit of Adam is due to a change in the update magnitude, or in the direction being closer to sign descent (Tieleman and Hinton, 2012; Balles and Hennig, 2018). We compare

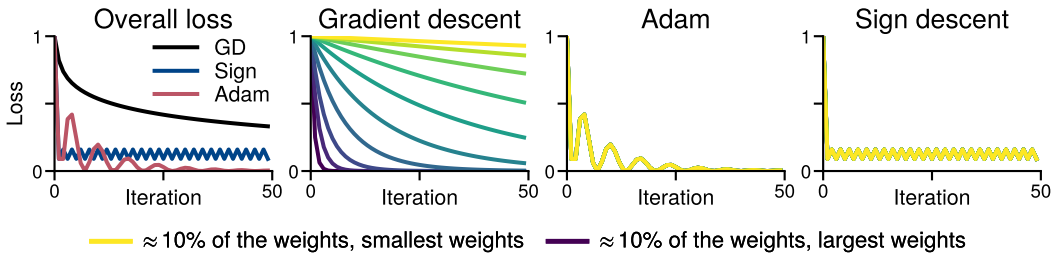

Figure 3: **Class-separation on the quadratic problem of Section 3.1 with weights $\pi_k \propto 1/k$.** GD fits functions with low weights more slowly, while Adam and sign descent have the same dynamics across all functions and all the lines overlap as every parameter w_i is initialized at $w_i = 1$.

GD, Adam, normalized GD and sign descent in Appendix E. Normalization and momentum help, but have less impact than changing the update direction; Sign descent and Adam perform similarly.

Upweighting low-frequency classes can help. Given our hypothesis that the performance gap is due to class imbalance, we expect interventions targeting imbalance to improve performance. In Appendix F, we show that upweighting the loss of low-frequency classes can improve the performance of SGD. While reweighting is not a complete solution as it changes the objective function, this experiment supports the hypothesis that the optimization difficulties are due to class imbalance.

3 An investigation on linear models

This section explores the effect of heavy-tailed class imbalance on softmax linear models to understand why GD becomes slow while Adam is less affected in Figure 2. In Section 3.1, we give a quadratic example where an imbalanced Hessian leads to a performance gap between GD and Adam. In Section 3.2, we show that class imbalance leads to such an imbalanced gradients and Hessians, correlated with class frequencies through an *assignment mechanism*, showing that this pattern emerges naturally. Finally in Section 3.3 we prove that, in continuous time and on a simple problem, GD is slow on low-frequency classes while sign descent is fast on all classes.

3.1 Intuition on a weighted quadratic problem

Consider the following problem, purposefully oversimplified to provide a high-level intuition about the optimization dynamics. Suppose we have c functions $f_1, ..., f_c$, corresponding to the losses for each class, that are on the same scale in the sense that gradient descent with step-size α makes fast progress on any f_i, for example $f_i(w) = \frac{1}{2}\|w\|^2$. Instead of running GD on each function independently, suppose we run GD on the weighted average $f(w_1, ..., w_c) = \sum_{i=1}^{c} \pi_i f_i(w_i)$ with positive weights $\pi_1 \geq ... \geq \pi_c$, $\sum_i \pi_i = 1$, corresponding to the class frequencies. If these weights span orders of magnitude, we expect a similar behavior as in Figures 1 and 2, as illustrated in Figure 3. GD makes slow progress on functions with low weights as the gradient w.r.t. w_k is scaled by π_k,

$$w_k^{(t)} = w_k^{(t-1)} - \alpha\pi_k f_k'(w_k^{(t-1)}) = (1 - \alpha\pi_k)^t w_k^{(0)}.$$

The problem is that we use the same step-size for functions with different scales. The slow convergence cannot be fixed by increasing the step-size, as $\alpha > 2/\pi_1$ causes instabilities on the "high-frequency class" f_1. On the other hand, the updates of Adam and sign descent are independent of π_k,

$$w_k^{(t)} = w_k^{(t-1)} - \alpha \frac{\pi_k f_k'(w_k^{(t-1)})}{|\pi_k f_k'(w_k^{(t-1)})|} = w_k^{(t-1)} - \alpha \operatorname{sign}(f_k'(w_k^{(t-1)})).$$

While sign descent or Adam with a fixed step-size need not converge and can oscillate around the minimum, they perform much better in early iterations, independently of π_k.

The imbalance in the weights π_i lead to an ill-conditioned problem, as the Hessian is $\operatorname{Diag}([\pi_1, ..., \pi_c])$. A common intuition for Adam is that the magnitude of the gradient is a good proxy for the diagonal Hessian (Duchi et al., 2011; Kingma and Ba, 2015), and a Newton step would take larger steps on coordinates with small π_k. While this connection does not hold in general (Kunstner et al., 2019), the approximation is not unreasonable here. The gradient is $[\pi_1 w_1, ..., \pi_c w_c]$ and if the weights π_i vary by orders of magnitude more than the parameters $|w_i|$, the gradient and Hessian diagonal will be correlated and lead to similar update directions.

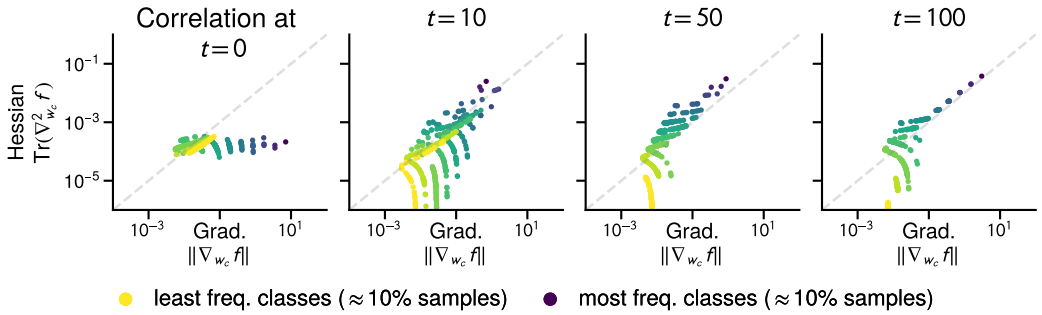

Figure 4: **The gradient norm and Hessian trace across blocks become correlated during training,** over the path taken by Adam in training the linear model of Figure 2. The blocks correspond to the rows $\mathbf{w}_1, ..., \mathbf{w}_c$ of the parameter matrix $\mathbf{W}$. The color indicates the class frequency, showing that lower (higher) frequency classes have smaller (larger) gradient norm and Hessian trace.

3.2 Correlations between the magnitude of the gradient and Hessian across coordinates

The caricature of the diagonal quadratic problem provides some intuition, but does not apply to the softmax linear model of Figure 2, which is neither quadratic nor separable. What is lacking to explain Adam's improved performance is an explanation for how this correlation between the gradient and Hessian arises in real problems. This feature has been observed on neural networks, but we do not yet know why it appears, even on the softmax linear problem. Nonetheless, a similar pattern emerges in the rows $\mathbf{w}_1, ..., \mathbf{w}_c$ of its parameter matrix $\mathbf{W}$; the magnitude of the gradient and Hessian across rows and the class frequencies become correlated during training due to class imbalance. In this section, we establish this observation empirically and provide a mechanism for how it emerges.

In Figure 4, we show the gradient norm against the Hessian trace for each block $\mathbf{w}_k$ throughout the trajectory of Adam on the softmax linear model of Figure 2. While there is no correlation at initialization, the gradient and Hessian blocks become correlated with class frequencies during training and become imbalanced. The diagonal blocks are orders of magnitude larger than off-diagonal blocks, as shown in Appendix H, indicating a weak dependence across blocks. Similar dynamics also occur with GD and across problems in the last layer of deep networks, shown in Appendix G.

To explain this behavior, we show that the impact of samples on the Hessian follows an *assignment mechanism*: if the model assigns samples to their correct class, the Hessian with respect to $\mathbf{w}_k$ is primarily influenced by samples from class k, leading to a correlation between the magnitude of the gradient, Hessian, and class frequencies. To capture this effect, we introduce some notation and a simplifying assumption. Suppose we have n samples with inputs $\mathbf{x}_i \in \mathbb{R}^d$ and labels $y_i \in [c]$, where class k has frequency $\pi_k = {}^{n_k}/_{n}$. The parameters of the linear model are $\mathbf{W} \in \mathbb{R}^{c \times d}$. We write $\mathbf{p}(\mathbf{x}) = \sigma(\mathbf{W}\mathbf{x})$ for the predicted probabilities where σ is the softmax, and summarize the data as

$$\bar{\mathbf{x}} = \tfrac{1}{n}\sum_{i=1}^{n} \mathbf{x}_i, \quad \bar{\mathbf{x}}^k = \tfrac{1}{n_k}\sum_{i:y_i=k} \mathbf{x}_i, \quad \bar{\mathbf{H}} = \tfrac{1}{n}\sum_{i=1}^{n} \mathbf{x}_i\mathbf{x}_i^\top, \quad \bar{\mathbf{H}}^k = \tfrac{1}{n_k}\sum_{i:y_i=k} \mathbf{x}_i\mathbf{x}_i^\top.$$

Assumption 1 (correct assignment)**.** The model correctly assigns samples to class k if it predicts k with non-negligible probability p on samples from that class ($\mathbf{p}(\mathbf{x}_i)_k = p = \omega({}^1/_c)$ for $\mathbf{x}_i$ from class $y_i = k$), and predicts k with near-random chance otherwise ($\mathbf{p}(\mathbf{x}_i)_k = O({}^1/_c)$ for $\mathbf{x}_i$ where $y_i \neq k$).

Proposition 2. *If initialized at $\mathbf{W}_0 = 0$, the gradient and Hessian of the loss $\mathcal{L}$ w.r.t. $\mathbf{w}_k$ are*

$$\nabla_{\mathbf{w}_k}\mathcal{L}(\mathbf{W}_0) = \pi_k\bar{\mathbf{x}}^k - \tfrac{1}{c}\bar{\mathbf{x}}, \qquad \nabla^2_{\mathbf{w}_k}\mathcal{L}(\mathbf{W}_0) = \tfrac{1}{c}\big(1-\tfrac{1}{c}\big)\bar{\mathbf{H}}, \tag{1}$$

During training, if the model correctly assigns samples to class k with probability p (Assumption 1),

$$\begin{aligned}\nabla_{\mathbf{w}_k}\mathcal{L} &= (1-p)\pi_k\,\bar{\mathbf{x}}^k + O\big(\tfrac{1}{c}\big),\\ \nabla^2_{\mathbf{w}_k}\mathcal{L} &= p(1-p)\pi_k\,\bar{\mathbf{H}}^k + O\big(\tfrac{1}{c}\big),\end{aligned} \quad \textit{and} \quad \|\nabla_{\mathbf{w}_k}\mathcal{L}\| \sim \left(\frac{1}{p}\frac{\|\bar{\mathbf{x}}^k\|}{\mathrm{Tr}(\bar{\mathbf{H}}^k)}\right)\mathrm{Tr}(\nabla^2_{\mathbf{w}_k}\mathcal{L}) \textit{ as } c\to\infty, \tag{2}$$

for classes where the frequency does not vanish too quickly, $\pi_k = \omega({}^1/_c)$.

The assumption that $c \to \infty$ is used to obtain a simple and interpretable equation in the correlation. In practice, $c > 10^3$ appears sufficient to make the dependence on π_k appear, as in Figure 4. We ignore off-diagonal blocks here, as they are orders of magnitude smaller than diagonal blocks (see Appendix H.1), and defer the derivation of the asymptotics to Appendix H.

At initialization, Equation (1) shows that the Hessian blocks are uniform across classes while the gradients depend on π_k, confirming the pattern observed at initialization in Figure 4. Equation (2) indicates a correlation between gradient norm and Hessian trace if classes have similar values of $\|\bar{\mathbf{x}}^k\|$, $\mathrm{Tr}(\bar{\mathbf{H}}^k)$ and predicted probabilities p, confirming the pattern observed during training in Figure 4.

This assignment mechanism explains how the gradient, Hessian and class probabilities can become correlated on the linear model. While the gradient does not directly approximate the Hessian, the main feature of the imbalance in both the gradient and Hessian comes from the weighting by the class frequencies $\pi_1, ..., \pi_c$. This correlation is not a global property of the problem, see Appendix G, but it appears during training if the optimization algorithm makes progress. While the normalization of Adam or sign descent is not designed to address class imbalance, it benefits from this property to make faster progress. Our results complement prior work on optimization with class imbalance on problems with few classes, which argued that the gradient is dominated by the majority class and is biased towards making progress on the majority class (Anand et al., 1993; Ye et al., 2021; Francazi et al., 2023). While this explains why GD might not make fast progress on rare classes, it is not clear why this would lead to slow performance on average. Our results show that, in addition to imbalances gradients, class imbalance leads to optimization difficulties through imbalanced Hessians.

3.3 Improvement of sign-based approaches over gradient descent

The above arguments provide a high-level intuition as to why the gradient might be a reasonable proxy for the Hessian, but it remains difficult to formally describe this effect and prove the benefits of Adam over GD. Doing so would require a fine-grained analysis of the dynamics, as the correlation only appears during training. To obtain a guarantee highlighting the benefit of sign-based methods, we consider a stripped-down problem where the only difficulty lies in the class imbalance:

Simple imbalanced setting. *Consider c classes with frequencies $\pi_1, ..., \pi_c$ where all samples from a class are the same, $\mathbf{x}_i = \mathbf{e}_k$ if $y_i = k$, where $\mathbf{e}_k$ is the kth standard basis vector in $\mathbb{R}^c$.*

This setting is trivial as it can be solved by taking one step of gradient descent with an arbitrarily large step-size. However, the dynamics with small step-sizes already exhibit the separation by class frequencies observed experimentally. We show that the continuous time variant of gradient descent, gradient flow, and sign descent as a proxy for Adam, obtain qualitatively different convergence rates.

Theorem 3. *On the* simple imbalanced setting*, gradient flow and continuous time sign descent initialized at $\mathbf{W} = 0$ minimize the loss of class k, $\ell_k(t) = -\log(\sigma(\mathbf{W}(t)\mathbf{e}_k)_k)$, at the rate*

$$\textit{Gradient flow:} \quad \ell_k(t) = \Theta(1/\pi_k t), \qquad \textit{Continuous time sign descent:} \quad \ell_k(t) = \Theta\big(e^{-ct}\big).$$

We defer to proof to Appendix I. The difference between the sublinear rate of gradient flow ($1/t$) and linear rate of sign descent (e^{-t}) is similar to existing results for overparameterized logistic regression, where normalized updates converge faster as they keep increasing the margin despite small gradients (Nacson et al., 2019). The novel element is that the convergence of gradient flow strongly depends on the class frequencies π, while the convergence of sign descent is independent of the class frequencies.

This setting is oversimplified and does not capture some features observed in our experiments. For example, in Theorem 3, the loss is monotonically decreasing for all classes, which does not hold in Figure 2. This setting is also biased towards sign descent, as the inputs are aligned with the basis vectors. Finally, the problem is inadequate to study large step-sizes, as it can be solved in one large step, but large step-sizes would lead to training instabilities and oscillations in the loss of frequent classes, as in Figure 2. Nevertheless, this result establishes the benefit of sign-based updates and we believe it captures the key difficulty encountered by GD under heavy-tailed class imbalance.

4 Conclusion

While class imbalance is unlikely to be the only problem in training large language models (see additional discussion in Appendix J), we have shown that heavy-tailed class imbalance leads to a performance gap between (S)GD and Adam. This effect appears across architectures and data types, but is most salient on language tasks which naturally exhibit heavy-tailed imbalance. As vision tasks are typically uniform, imbalance is a key differentiating feature of the training difficulties in language tasks. The correlation between gradient and Hessian blocks that occurs due to class imbalance provides a simple property that justifies the intuition that Adam can "adapt to curvature". We provide an explanation for how this correlation arises and prove on a simple problem that GD performs poorly on low-frequency classes while sign descent is unaffected by class frequencies.

References

Kwangjun Ahn, Xiang Cheng, Minhak Song, Chulhee Yun, Ali Jadbabaie, and Suvrit Sra (2023). "Linear attention is (maybe) all you need (to understand transformer optimization)". In: *arXiv preprint* arXiv:2310.01082.

Rangachari Anand, Kishan G. Mehrotra, Chilukuri K. Mohan, and Sanjay Ranka (1993). "An improved algorithm for neural network classification of imbalanced training sets". In: *IEEE Transactions on Neural Networks* 4.6, pp. 962–969.

Jimmy Ba, Jamie Ryan Kiros, and Geoffrey E. Hinton (2016). "Layer Normalization". In: *Neural Information Processing Systems (NeurIPS), Deep Learning Symposium.*

Lukas Balles and Philipp Hennig (2018). "Dissecting Adam: The Sign, Magnitude and Variance of Stochastic Gradients". In: *International Conference on Machine Learning (ICML)*. Vol. 80, pp. 413–422.

Lucas Beyer, Xiaohua Zhai, and Alexander Kolesnikov (2022). "Better plain ViT baselines for ImageNet-1k". In: *CoRR* abs/2205.01580.

Alberto Bietti, Vivien Cabannes, Diane Bouchacourt, Herve Jegou, and Leon Bottou (2023). "Birth of a Transformer: A Memory Viewpoint". In: *Neural Information Processing Systems (NeurIPS)*.

Tom B. Brown et al. (2020). "Language Models are Few-Shot Learners". In: *Neural Information Processing Systems (NeurIPS)*.

Michael Crawshaw, Mingrui Liu, Francesco Orabona, Wei Zhang, and Zhenxun Zhuang (2022). "Robustness to Unbounded Smoothness of Generalized SignSGD". In: *Neural Information Processing Systems (NeurIPS)*.

Jia Deng, Wei Dong, Richard Socher, Li-Jia Li, Kai Li, and Li Fei-Fei (2009). "ImageNet: A large-scale hierarchical image database". In: *Conference on Computer Vision and Pattern Recognition (CVPR)*.

John C. Duchi, Elad Hazan, and Yoram Singer (2011). "Adaptive Subgradient Methods for Online Learning and Stochastic Optimization". In: *Journal of Machine Learning Research (JMLR)* 12, pp. 2121–2159.

Vitaly Feldman (2020). "Does learning require memorization? a short tale about a long tail". In: *Symposium on Theory of Computing (STOC)*, pp. 954–959.

Emanuele Francazi, Marco Baity-Jesi, and Aurélien Lucchi (2023). "A Theoretical Analysis of the Learning Dynamics under Class Imbalance". In: *International Conference on Machine Learning (ICML)*. Vol. 202, pp. 10285–10322.

Philip Gage (1994). "A new algorithm for data compression". In: *C Users Journal* 12.2, pp. 23–38.

Nikhil Ghosh, Song Mei, and Bin Yu (2022). "The Three Stages of Learning Dynamics in High-dimensional Kernel Methods". In: *International Conference on Learning Representations (ICLR)*.

Thamme Gowda and Jonathan May (2020). "Finding the Optimal Vocabulary Size for Neural Machine Translation". In: *Findings of the Association for Computational Linguistics (EMNLP)*, pp. 3955–3964.

Bobby He, James Martens, Guodong Zhang, Aleksandar Botev, Andrew Brock, Samuel L. Smith, and Yee Whye Teh (2023). "Deep Transformers without Shortcuts: Modifying Self-attention for Faithful Signal Propagation". In: *International Conference on Learning Representations (ICLR)*.

Kaiming He, Xiangyu Zhang, Shaoqing Ren, and Jian Sun (2016). "Deep Residual Learning for Image Recognition". In: *Conference on Computer Vision and Pattern Recognition (CVPR)*, pp. 770–778.

Abdolhossein Hoorfar and Mehdi Hassani (2008). "Inequalities on the Lambert function and hyper-power function". In: *Journal of Inequalities in Pure and Applied Mathematics* 9.2.

Sergey Ioffe and Christian Szegedy (2015). "Batch Normalization: Accelerating Deep Network Training by Reducing Internal Covariate Shift". In: *International Conference on Machine Learning (ICML)*. Vol. 37, pp. 448–456.

Kaiqi Jiang, Dhruv Malik, and Yuanzhi Li (2022). "How Does Adaptive Optimization Impact Local Neural Network Geometry?" In: *arXiv preprint* arXiv:2211.02254.

Diederik P. Kingma and Jimmy Ba (2015). "Adam: A Method for Stochastic Optimization". In: *International Conference on Learning Representations (ICLR)*.

Taku Kudo (2018). "Subword Regularization: Improving Neural Network Translation Models with Multiple Subword Candidates". In: *Annual Meeting of the Association for Computational Linguistics (ACL)*, pp. 66–75.

Frederik Kunstner, Jacques Chen, Jonathan Wilder Lavington, and Mark Schmidt (2023). "Noise is not the main factor behind the gap between SGD and Adam on transformers, but sign descent might be". In: *International Conference on Learning Representations (ICLR)*.

Frederik Kunstner, Philipp Hennig, and Lukas Balles (2019). "Limitations of the empirical Fisher approximation for natural gradient descent". In: *Neural Information Processing Systems (NeurIPS)*, pp. 4158–4169.

Yann LeCun, Léon Bottou, Yoshua Bengio, and Patrick Haffner (1998). "Gradient-Based Learning Applied to Document Recognition". In: *Proceedings of the IEEE*. Vol. 86. 11, pp. 2278–2324.

Liyuan Liu, Xiaodong Liu, Jianfeng Gao, Weizhu Chen, and Jiawei Han (2020). "Understanding the Difficulty of Training Transformers". In: *Conference on Empirical Methods in Natural Language Processing (EMNLP)*, pp. 5747–5763.

Mitchell P. Marcus, Beatrice Santorini, and Mary Ann Marcinkiewicz (1993). "Building a Large Annotated Corpus of English: The Penn Treebank". In: *Computational Linguistics* 19.2, pp. 313–330.

Kevin Meng, David Bau, Alex Andonian, and Yonatan Belinkov (2022). "Locating and editing factual associations in GPT". In: *Neural Information Processing Systems (NeurIPS)*.

Stephen Merity, Caiming Xiong, James Bradbury, and Richard Socher (2017). "Pointer Sentinel Mixture Models". In: *International Conference on Learning Representations (ICLR)*.

Eric J. Michaud, Ziming Liu, Uzay Girit, and Max Tegmark (2023). "The quantization model of neural scaling". In: *Neural Information Processing Systems (NeurIPS)*.

Mor Shpigel Nacson, Jason D. Lee, Suriya Gunasekar, Pedro Henrique Pamplona Savarese, Nathan Srebro, and Daniel Soudry (2019). "Convergence of Gradient Descent on Separable Data". In: *International Conference on Artificial Intelligence and Statistics (AISTATS)*. Vol. 89, pp. 3420–3428.

Preetum Nakkiran, Behnam Neyshabur, and Hanie Sedghi (2021). "The deep bootstrap framework: Good online learners are good offline generalizers". In: *International Conference on Learning Representations (ICLR)*.

Lorenzo Noci, Sotiris Anagnostidis, Luca Biggio, Antonio Orvieto, Sidak Pal Singh, and Aurélien Lucchi (2022). "Signal Propagation in Transformers: Theoretical Perspectives and the Role of Rank Collapse". In: *Neural Information Processing Systems (NeurIPS)*.

Antonio Orvieto, Jonas Kohler, Dario Pavllo, Thomas Hofmann, and Aurélien Lucchi (2022). "Vanishing Curvature in Randomly Initialized Deep ReLU Networks". In: *International Conference on Artificial Intelligence and Statistics (AISTATS)*. Vol. 151, pp. 7942–7975.

Yan Pan and Yuanzhi Li (2023). *Toward Understanding Why Adam Converges Faster Than SGD for Transformers*. NeurIPS 2022 Workshop on Optimization for Machine Learning. arXiv/2306.00204.

Adam Paszke et al. (2019). "PyTorch: An Imperative Style, High-Performance Deep Learning Library". In: *Neural Information Processing Systems (NeurIPS)*, pp. 8024–8035.

Steven T. Piantadosi (2014). "Zipf's word frequency law in natural language: A critical review and future directions". In: *Psychonomic bulletin & review* 21, pp. 1112–1130.

Alec Radford, Jeff Wu, Rewon Child, David Luan, Dario Amodei, and Ilya Sutskever (2019). *Language Models are Unsupervised Multitask Learners*. Tech. Report.

Elan Rosenfeld and Andrej Risteski (2023). "Outliers with Opposing Signals Have an Outsized Effect on Neural Network Optimization". In: *arXiv preprint* arXiv/2311.04163.

Shiori Sagawa, Aditi Raghunathan, Pang Wei Koh, and Percy Liang (2020). "An investigation of why overparameterization exacerbates spurious correlations". In: *International Conference on Machine Learning (ICML)*.

Robin M. Schmidt, Frank Schneider, and Philipp Hennig (2021). "Descending through a Crowded Valley - Benchmarking Deep Learning Optimizers". In: *International Conference on Machine Learning (ICML)*. Vol. 139, pp. 9367–9376.

Rico Sennrich, Barry Haddow, and Alexandra Birch (2016). "Neural Machine Translation of Rare Words with Subword Units". In: *Annual Meeting of the Association for Computational Linguistics (ACL)*.

Nitish Srivastava, Geoffrey E. Hinton, Alex Krizhevsky, Ilya Sutskever, and Ruslan Salakhutdinov (2014). "Dropout: a simple way to prevent neural networks from overfitting". In: *Journal of Machine Learning Research (JMLR)* 15.1, pp. 1929–1958.

Tijmen Tieleman and Geoffrey Hinton (2012). *RMSPROP: Divide the gradient by a running average of its recent magnitude*. Lecture notes
http://www.cs.toronto.edu/~tijmen/csc321/slides/lecture_slides_lec6.pdf.

Hugo Touvron, Matthieu Cord, Matthijs Douze, Francisco Massa, Alexandre Sablayrolles, and Hervé Jégou (2021). "Training data-efficient image transformers & distillation through attention". In: *International Conference on Machine Learning (ICML)*. Vol. 139, pp. 10347–10357.

Ashish Vaswani, Noam Shazeer, Niki Parmar, Jakob Uszkoreit, Llion Jones, Aidan N. Gomez, Lukasz Kaiser, and Illia Polosukhin (2017). "Attention is All you Need". In: *Neural Information Processing Systems (NeurIPS)*, pp. 5998–6008.

Kevin Ro Wang, Alexandre Variengien, Arthur Conmy, Buck Shlegeris, and Jacob Steinhardt (2023). "Interpretability in the Wild: a Circuit for Indirect Object Identification in GPT-2 Small". In: *International Conference on Learning Representations (ICLR)*.

Jake Ryland Williams, Paul R. Lessard, Suma Desu, Eric M. Clark, James P. Bagrow, Christopher M. Danforth, and Peter Sheridan Dodds (2015). "Zipf's law holds for phrases, not words". In: *Scientific reports* 5.1, p. 12209.

Han-Jia Ye, De-Chuan Zhan, and Wei-Lun Chao (2021). "Procrustean Training for Imbalanced Deep Learning". In: *International Conference on Computer Vision (ICCV)*, pp. 92–102.

Jingzhao Zhang, Tianxing He, Suvrit Sra, and Ali Jadbabaie (2020a). "Why Gradient Clipping Accelerates Training: A Theoretical Justification for Adaptivity". In: *International Conference on Learning Representations (ICLR)*.

Jingzhao Zhang, Sai Praneeth Karimireddy, Andreas Veit, Seungyeon Kim, Sashank J. Reddi, Sanjiv Kumar, and Suvrit Sra (2020b). "Why are Adaptive Methods Good for Attention Models?" In: *Neural Information Processing Systems (NeurIPS)*, pp. 15383–15393.

Vilém Zouhar, Clara Meister, Juan Luis Gastaldi, Li Du, Mrinmaya Sachan, and Ryan Cotterell (2023). "Tokenization and the Noiseless Channel". In: *Annual Meeting of the Association for Computational Linguistics (ACL)*, pp. 5184–5207.

Supplementary Material

A Experimental details

This section documents the datasets, models, software, and experimental setup. The code is available at https://github.com/fkunstner/class-imbalance-sgd-adam.

A.1 Datasets

- **WikiText-103** (Merity et al., 2017), using sequences of $1\,024$ tokens and the BPE tokenizer (Sennrich et al., 2016), with a vocabulary of size $50\,608$.
- **WikiText-2** (Merity et al., 2017) is used in Appendix A.7 to illustrate that other combinations of datasets and tokenizers lead to heavy-tailed distributions.
- **PTB** (Marcus et al., 1993), using sequences of 35 tokens built from a word-based tokenizer (`basic_english` provided by `torchtext`), for a vocabulary of size $9\,920$. For deterministic runs, we use the validation set as a reduced training set, labeled **TinyPTB**.
- **MNIST** (LeCun et al., 1998).
- **ImageNet** (Deng et al., 2009).

A.2 Custom datasets

- **The Random Heavy-Tailed Labels dataset** is a synthetic dataset exhibiting heavy-tailed class imbalance. The number of samples per class and the number of classes are picked to approximate a power-law distribution. We create m "groups" of classes, where each class within a group has the same relative frequency;

  $$\underbrace{1 \text{ class with } 2^m \text{ samples},}_{\text{group } 1} \quad \underbrace{2 \text{ classes with } 2^{m-1} \text{ samples},}_{\text{group } 2} \quad \ldots, \quad \underbrace{2^{m-1} \text{ classes with } 2 \text{ samples.}}_{\text{group } m}$$

  The inputs are drawn from a uniform distribution on $[0, 1]$, independently of the class label. The inputs are in $d = (m+1)\,2^m$ dimensions, the number of samples is $n = m\,2^m$ and the number of classes is $c = 2^{m+1} - 1$. We use two variants of the datasets; a large one in Figure 2, Appendix E ($m = 11, n = 22\,528, d = 24\,576, c = 4\,095$) and a small one in Appendix C ($m = 8, n = 2\,048, d = 2\,304, c = 511$).
- **The Barcoded MNIST dataset** is a modified variant of MNIST. We start with 50k examples from the original MNIST dataset across 10 classes, and create $51\,200$ ($5 \times 10 \times 2^{10}$) new images. The new examples are copies of existing image with an added "barcode", a 10-bit number encoded in a corner of the image, as in the examples below. The class label is a combination of the original class and this barcode.

  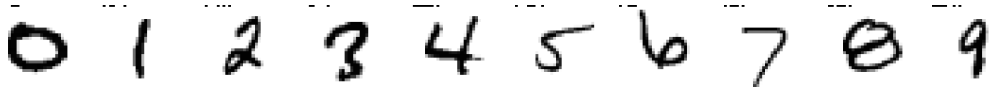

  The **Barcoded-only** dataset contains 10×2^{10} classes with 5 samples each. To obtain an imbalanced dataset, we combine the barcoded images with the original samples from the MNIST dataset to get $101\,200$ examples spread across $10\,250$ ($10 \times 2^{10} + 10$) classes classes; $10\,240$ with 5 examples per class and 10 classes with $\approx 5k$ examples per class, labeled **MNIST+Barcoded**
- **The Heavy Tailed ImageNet** dataset is a subset of ImageNet (Deng et al., 2009), subsampled to exhibit heavy-tailed class imbalance. We sort the original 1000 classes by frequency and sample $\lceil \frac{1300}{k} \rceil$ images from the kth class, leading to $n = 10\,217$ samples.
- **The small ImageNet** dataset is a uniform subset of ImageNet to contrast the with the heavy tailed variant. We sample 10 images per class to get $n = 10\,000$ samples.

A.3 Models

- **The 2-layer transformer** used in Appendix D is a transformer Vaswani et al. (2017), based on the PyTorch implementation of `TransformerEncoderLayer` (Paszke et al., 2019).

  $$\text{Embedding} \to 2\times \text{ [Attention} \to \text{Linear} \to \text{ReLU} \to \text{Linear]} \to \text{Classifier.}$$

  The model includes LayerNorm, dropout, and skip connections (He et al., 2016; Ba et al., 2016; Srivastava et al., 2014). The embedding dimension and width of the linear layers is 1000 and the attention modules use 4 heads.

- **The simplified transformer** used in Figure 17 and Appendix D does not use encoder blocks, and only uses attention:

  $$\text{Embedding} \to \text{Attention} \to \text{Classifier.}$$

  We remove LayerNorm, dropout, and the block [Linear $\to$ ReLU $\to$ Linear] containing the non-linearity. In Figure 17, we freeze the embedding and attention layers at initialization, and only the last classification layer is trained. The model is then a linear model on a fixed feature transformation.

- **The GPT2-Small** model (Radford et al., 2019) is used in Figure 1. The blocks includes LayerNorm, residual connections, and dropout on the embedding and dense layers. We use sinusoidal encoding as in the transformer architecture (Vaswani et al., 2017). The embedding dimension is 768, the width of the intermediate layers is 3072, and we use 12 encoder blocks with 12 self attention heads.

- **The convolutional network** used in Figure 7 and Appendix B is a 2-layer convolution

  $$\text{Conv} \to \text{Relu} \to \text{MaxPool} \to \text{Conv} \to \text{Relu} \to \text{MaxPool} \to \text{Linear}$$

- **The linear model** used in Figures 2 and 4 and Appendix E uses a bias vector.

- **The ResNet18** model (He et al., 2016) is used in Figure 8. Additionally, a variant replacing the BatchNorm layers with LayerNorm is used in Appendix B.

- **The SimpleViT** model (Beyer et al., 2022) used in Appendix B follows the architecture of a ViT-S/16 (Touvron et al., 2021), based on the `vit-pytorch` implementation (`https://github.com/lucidrains/vit-pytorch` `v1.6.5`).

A.4 Training procedures

Our primary focus is on the performance of the optimizers on the training error, using the simplest training procedure possible. We use a constant step-size throughout training, set by grid search. We start with a sparse grid of powers of 10 $[10^{-6}, 10^{-2}, ..., 10^{1}]$ and increase the density to half-powers around the best step-size. The step-size is selected to minimize the maximum over 3 seeds of the training loss at the end of training. For some settings, this selection still produces runs that are unstable; the training loss is the smallest at the end but oscillates a lot during training, reaching loss values that are worse than at initialization. For those runs, we use the next smaller step-size, which has similar performance but is more stable.

We use gradient accumulation (computing the gradient through multiple passes) to achieve the following batch sizes;

- The large transformer experiment in Figure 1 uses mini-batches of 512 sequences of 1024 tokens.
- The stochastic experiments with a smaller transformer in Appendix D uses mini-batches of 512 sequences of 35 tokens.
- Both ResNet18 variants and the Simple Vision Transformer were trained using mini-batches of 1024. The training images were normalized and randomly cropped to 224×224 pixels as is standard for ImageNet training.
- Other experiments use the entire dataset to compute updates

Our experiments ran on a cluster using a mix of A100, P100, V100, and H100 GPUs. The large scale experiment in Figure 1 took 3 days on a H100, while all other experiments ran in 2–8 hours. The total amount of compute used for this project is ≈3 GPU-years, including preliminary experiments.

A.5 Summary of settings used

Table 1: Summary of models, datasets and batch-size used

Model	Dataset	Batch size	Used in
GPT2-Small	WT103	512	Figure 1 and Figure 6
2-layer transformer	PTB	512	Figures 15, 21 and 25
1-layer transformer	TinyPTB	Full	Figures 16 and 19
1-layer transformer	TinyPTB	Full	Figure 17 (last layer only)
CNN	Barcoded MNIST	Full	Figure 12
CNN	MNIST	Full	Figures 7 and 12
CNN	MNIST+Barcoded	Full	Figures 7, 12, 20, 21 and 23
Linear	Random HT labels, m=11	Full	Figures 2, 4, 18, 21, 22, 26 and 27
Linear	Random HT labels, m=7	Full	Figures 13 and 14
Simple ViT	ImageNet	1024	Figure 10
ResNet18	Small and HT ImageNet	1024	Figures 8, 21 and 24
ResNet18+LN	Small and HT ImageNet	1024	Figure 9
Simple ViT	Small and HT ImageNet	1024	Figure 11

A.6 Optimization algorithms

Given momentum buffers m_t initialized at $m_0 = 0$ and a (possibly) stochastic gradient $\tilde{g}_t$, we implement the update of GD, normalized GD and sign descent with heavy-ball momentum as

$$m_t = \beta m_{t-1} + d_t,$$
$$x_{t+1} = x_t - \alpha m_t,$$
$$\text{with } d_t = \begin{cases} \tilde{g}_t & \text{for gradient descent,} \\ \tilde{g}_t / \|\tilde{g}_t\|_2 & \text{for normalized GD,} \\ \operatorname{sign}(\tilde{g}_t) & \text{for sign descent.} \end{cases}$$

For Adam, we use the standard implementation in PyTorch (Paszke et al., 2019).

A.7 Class distribution for common datasets and tokenizers

Figure 5 provides additional examples of the heavy-tailed distribution of tokens using the basic english tokenizer in `torchtext` (Paszke et al., 2019), Byte-Pair Encoding (BPE, Sennrich et al., 2016; Gage, 1994) and Unigram (Kudo, 2018) on the PTB and WikiText-2 datasets. The relationship between the relative frequency rank k and and the relative frequency π_k is roughly $\pi_k \propto 1/k$.

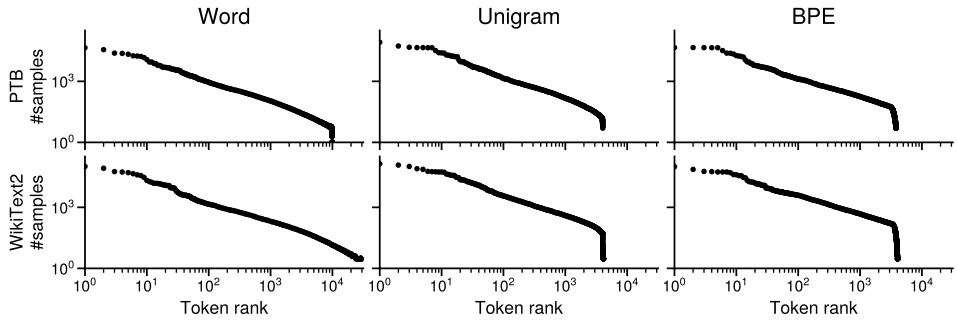

Figure 5: **Different tokenizers and datasets lead to heavy-tailed token distributions.** Comparison of word and subword tokenization (BPE, Unigram) on the PTB and WikiText2 datasets.

A.8 Validation loss

In Figure 6, we show the validation error on the same problem as Figure 1, training GPT2-Small on WikiText-103. The validation loss exhibits the same separation across class frequencies, and the faster progress of Adam on low-frequency classes is also visible. While this trend does not hold for all the settings we investigate, as some settings use smaller datasets and deterministic training to isolate the source of the training difficulties, the benefit of Adam on low-frequency classes does not immediately lead to overfitting.

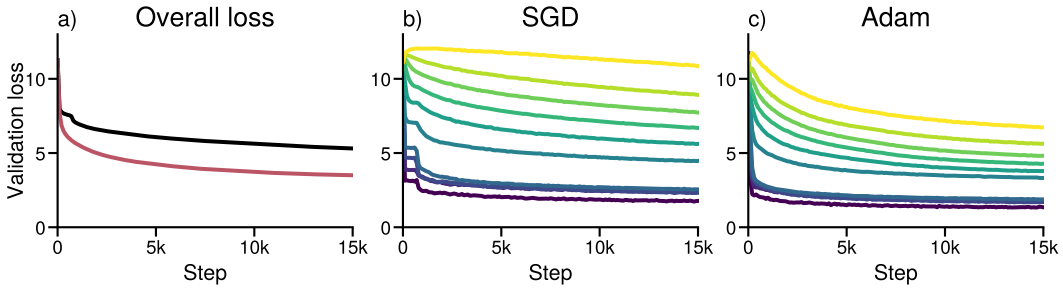

Figure 6: **The class-separation behavior of Figure 1 holds on the validation loss.** Same experiment as Figure 1, training GPT2-Small on WikiText-103, but showing the validation loss. (a) Distribution of the classes sorted by class frequency, split into groups corresponding to ≈10% of the data. (b) Overall validation loss. (c, d) Validation loss for each group using SGD and Adam. SGD makes little to no progress on low-frequency classes while Adam makes progress on all groups. (b) is the average of (c, d) for the respective optimizer.

B Heavy-tailed imbalance on vision datasets

This section gives additional results on vision tasks to complement Section 2.1.

- Figure 7 shows a similar behavior on a ResNet18 with LayerNorm instead of BatchNorm.
- Figure 9 shows a similar behavior on a ResNet18 with LayerNorm instead of BatchNorm.
- Figure 10 shows a similar behavior with a vision transformer.
- Figure 12 confirms that GD can solve the barcoded MNIST variant without imbalance.

B.1 LeNet5 + MNIST

We first use a CNN on a variant of MNIST with heavy-tailed class imbalance. We augment the dataset to have two equally-sized groups of classes with a relative frequency difference of 1000. The first group consists of the original 10 classes with ≈5k samples/class. For the second, we create ≈10k new classes with 5 samples/class. We create new classes by copying existing images and adding a "barcode" in a corner of the image, see Appendix A. The performance of GD and Adam is shown in Figure 7. On the original MNIST dataset, both optimizers drive the loss to 0. But on the imbalanced variant, GD makes almost no progress on half of the data corresponding to the low-frequency classes and progress stalls, while Adam makes progress on both groups.

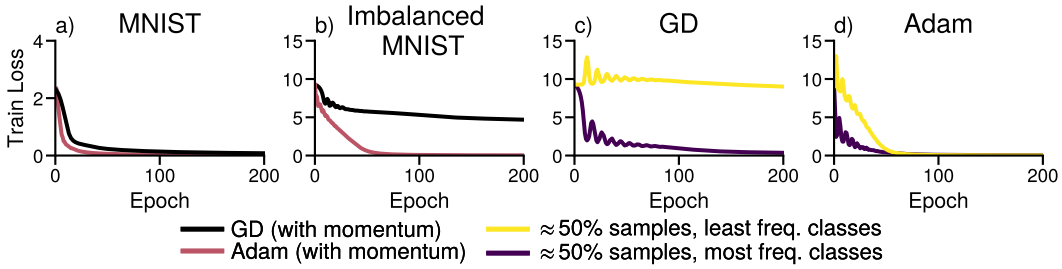

Figure 7: **Adam outperforms SGD for training a CNN under heavy-tailed class labels. (a)** Performance on the MNIST dataset. **(b)** Performance on a modified MNIST with two groups of classes. The first group consists of the 10 original classes with ≈ 5k samples each, while the second consists of ≈10k added classes with 5 examples each. **(c, d)** Performance of GD and Adam on the two groups.

B.2 ResNet + ImageNet

In Figure 8, we train a ResNet18 on an imbalanced subset of ImageNet, where classes where subsampled by $\pi_k \propto 1/k$, and are compared against a uniform subset of ImageNet with the same number of samples.

In Figure 9, we reproduce the setting of Figure 8, but replaces the normalization layers with LayerNorm (Ba et al., 2016) instead of BatchNorm (Ioffe and Szegedy, 2015). We observe a similar pattern as in Figure 8. Although Adam slightly outperforms SGD on the uniform dataset, the performance gap grows on the imbalanced one.

B.3 Vision transformer + ImageNet

In Figure 10, we train a vision transformer on the ImageNet dataset, without subsampling, to confirm that the training behavior is similar. While vision transformers might require more data or regularization than their ResNet counterparts to achieve comparable generalization performance, the optimization problem does not appear to be more difficult for SGD than for Adam.

In Figure 11, we train the same vision transformer on the uniform and imbalanced subsets of ImageNet. As in prior experiments with vision data, the performance of Adam appears unaffected by the change in class frequencies while the performance of SGD degrades.

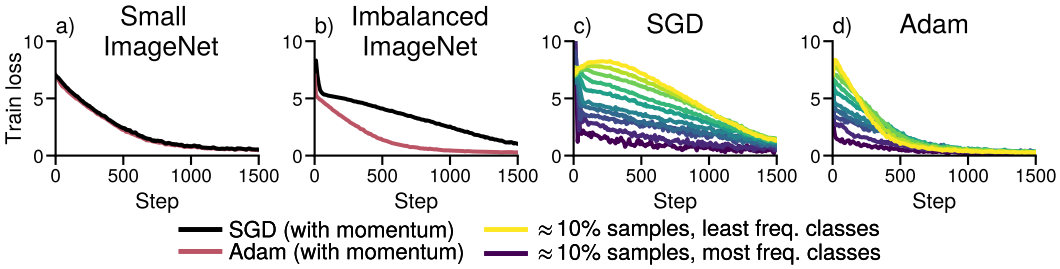

Figure 8: **Adam outperforms SGD for training a ResNet under heavy-tailed class labels. (a)** Performance on a subset of ImageNet and **(b)** an imbalanced subset of ImageNet with class frequencies $\pi_k \propto 1/k$. **(c, d)** Performance of GD and Adam on groups corresponding to $\approx 10\%$ of the data.

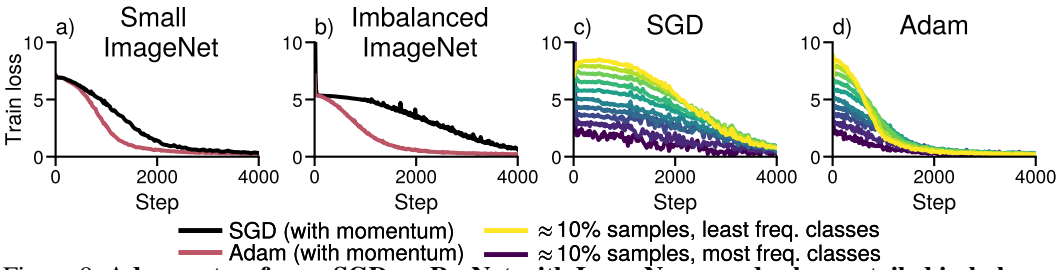

Figure 9: **Adam outperforms SGD on ResNet with LayerNorm under heavy-tailed imbalance.** (a) Performance on a uniform subset of ImageNet (b) and on an imbalanced subset with class frequencies $\pi_k \propto 1/k$. (c, d) Performance of GD and Adam across frequencies.

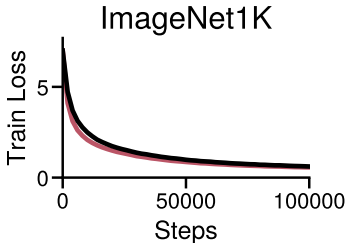

Figure 10: **Adam and SGD perform similarly training a Vision Transformer with balanced Classes.** Training loss on the full ImageNet dataset (without subsampling). There is little performance in training performance.

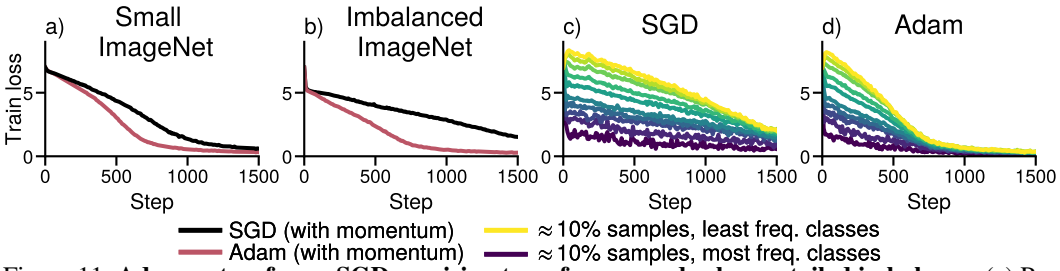

Figure 11: **Adam outperforms SGD on vision transformer under heavy-tailed imbalance.** (a) Performance on a uniform subset of ImageNet (b) and on an imbalanced subset with class frequencies $\pi_k \propto 1/k$. (c, d) Performance of GD and Adam across frequencies.

B.4 Sanity checks on Barcoded MNIST

Figure 7 in Section 2.1 showed that the performance gap between GD and Adam on the imbalanced variant of MNIST with barcoded images is larger than on plain MNIST. In this section, we verify that the training difficulties encountered on the CNN on the imbalanced MNIST dataset of Figure 7 are indeed due to class imbalance. As we create new images and new classes by adding a barcode in the corner of existing images, it could be that the dataset becomes harder to fit.

In Figure 12, we run Adam and GD to train the same network on the MNIST dataset only, the barcoded-only subset of the imbalanced MNIST and the combination of the two, leading to an imbalanced dataset. While Adam is faster GD on the barcoded-only dataset, both algorithms reach negligible error within 200 steps. In contrast, on the combined imbalanced dataset MNIST+Barcoded, GD fails to make progress on the low-frequency classes and stalls.

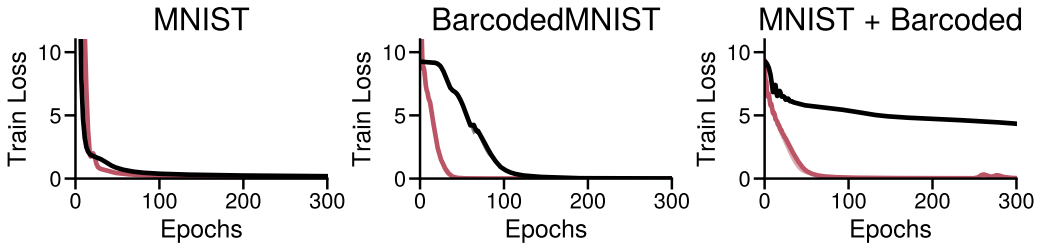

Figure 12: **GD optimizes on balanced barcoded data.** Training a CNN on only the barcoded portion of the data, which has balanced classes. While Adam is slightly faster, both optimizers reach negligible error within 200 steps. As the level of imbalance is increased, GD performs increasingly worse than Adam.

C Additional examples on linear models with class imbalance

In Section 2.2, we showed that GD already becomes slow in the presence of class imbalance. In this section, we give additional details. We discuss the impact of the input distribution, as class imbalance alone is technically not sufficient to make GD slow, and show that GD eventually does converge.

C.1 Impact of input distribution

Imbalance alone is not sufficient to induce slow performance of GD on low-frequency classes. It is possible to generate a dataset with heavy-tailed class imbalance where GD fits all classes fast, by making the inputs $\mathbf{x}_i$ (close to) orthogonal, $\langle \mathbf{x}_i, \mathbf{x}_j \rangle \approx 0$ for $i \neq j$.

In the proof of Theorem 3 in Appendix I, we use the independence across classes to show that the classes are learned at a rate $\propto 1/\pi_k$. If *all* the samples are orthogonal, $\langle \mathbf{x}_i, \mathbf{x}_j \rangle = 0$ for every i, j, a similar decomposition can show that each sample will be learned independently of all the other, at a speed that does not depend on a class frequency.

Note that it is also not necessary for all samples to be independent of each other. In the simple setting used in Theorem 3, samples from the same class are collinear while samples from separate class are independent A mixture model where samples from the same class are aligned ($|\langle \mathbf{x}_i, \mathbf{x}_j \rangle| > \delta$ if $y_i = y_j$) but independent otherwise ($|\langle \mathbf{x}_i, \mathbf{x}_j \rangle| \leq \epsilon$ if $y_i \neq y_j$), as the setting of Feldman (2020) would also exhibit class separation.

To avoid this issue in Figure 2, we draw the inputs from a high-dimensional uniform distribution on $[0, 1]^d$, ensuring that for any two samples $\mathbf{x}_i, \mathbf{x}_j$, $\langle \mathbf{x}_i, \mathbf{x}_j \rangle > 0$. If we were to sample data from $\mathcal{N}(0, 1)^d$ in sufficiently high dimension, the samples can be independent enough to avoid the slowdown due to class imbalance. We illustrate this in Figure 13, where we use a smaller synthetic data with inputs drawn from $\mathcal{N}(1, 1)$ (left) and $\mathcal{N}(0, 1)$ (right). The zero-mean data, which is be approximately orthogonal as $d > n$, does not exhibit a slow progress on low-frequency classes.

Note that if the linear model uses a bias term, this effectively makes the samples more aligned, as it is equivalent to adding a dimension to the input data where each sample has the same value. The behavior of GD on aligned data appears to be a better representation of the behavior of GD on language transformers, as we observe a performance separation per class frequency on GD, even when tuning only the last layer of a language transformer in Figure 17. Although the embedding are initialized to be zero-mean Gaussian noise, the embedding representation of the tokens in transformer are aligned, and this alignment increases with depth (Noci et al., 2022, e.g.).

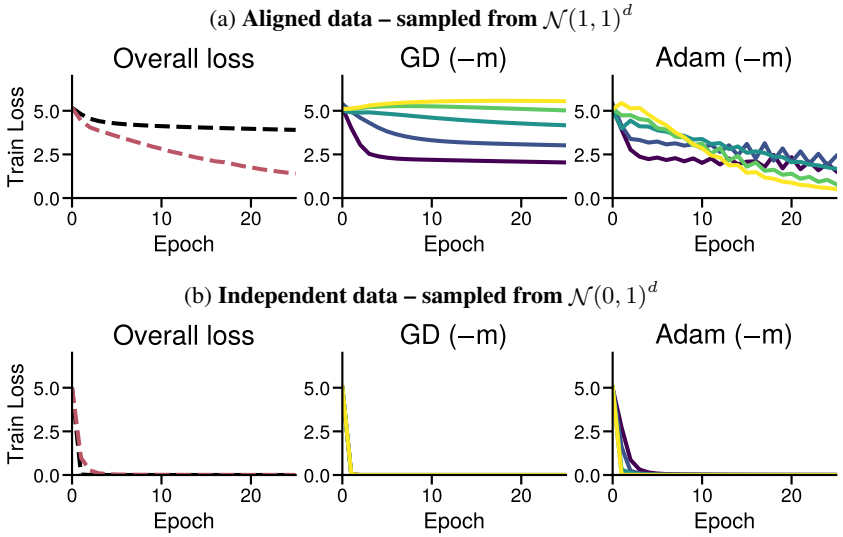

Figure 13: **The distribution of the inputs can have a large impact on the performance.** Linear softmax regression on the Random Heavy-Tailed Labels dataset, but with inputs sampled from $\mathcal{N}(1, 1)$ (a) and $\mathcal{N}(0, 1)$ (b).

C.2 An early iteration problem

The observed behavior that GD is slower than Adam at fitting the low-frequency classes, might make it seem that GD does not fit the low-frequency classes at all. Of course, when run for longer, GD converges and fits all classes, as shown in Figure 14. This highlight that the difference between the algorithms is primarily a difference at the start of training. However, this "start" can be quite long on large problems, as in the transformer of Figure 1, the average loss on 10% of the data corresponding to the least frequent classes is still higher than at initialization after 15k steps.

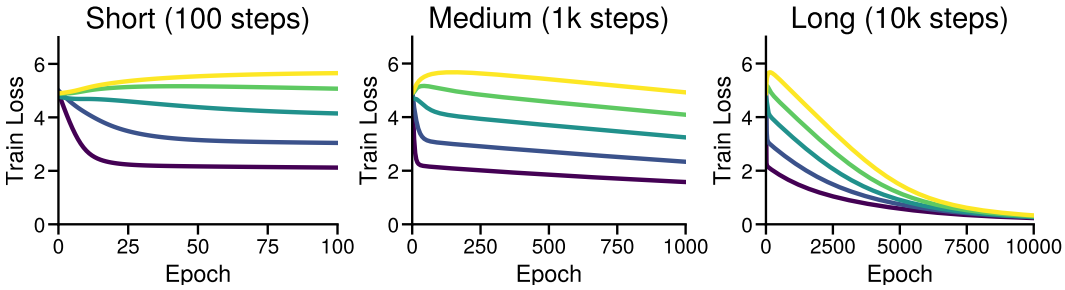

Figure 14: **Training with GD eventually drives the loss down for all classes.** Training loss over time, with the same step-size, for different time horizons (100, 1k, 10k full gradient steps). GD eventually drives the loss down for all classes, but the loss for the least-frequent classes only goes below the loss at initialization after 1k steps.

D Stochasticity is not necessary to reproduce the gap

In Section 2.3, we argued that the qualitatively different behavior on low-frequency classes between SGD and Adam in Figure 1 is not due to stochasticity. In this section, we provide additional results showing that this behavior appears across multiple batch sizes on language transformers of different sizes and that it can be reproduced in the deterministic setting.

In Figure 15, we show that a similar qualitative behavior appears when training a smaller model (2-layer transformer) on a smaller dataset (PTB). In Figure 16, we repeat the experiment with a 1-layer transformer, trained in full batch on TinyPTB (the validation set of PTB). The separation between GD and Adam on low-frequency classes in the deterministic settings is also visible in Figures 2, 4, 7 and 17 in the main paper. These results indicate that stochasticity it is not necessary to reproduce the behavior observed in Figure 1.

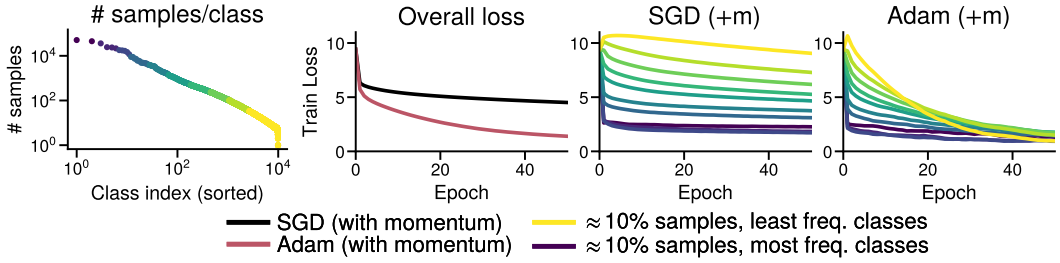

Figure 15: **Similar behavior as Figure 1 on a smaller problem.** Training a 2-layer transformer on PTB with Adam and SGD using larger batch-sizes. As in Figure 1, SGD makes little to no progress on low-frequency classes while Adam makes progress on all subsets. **(a)** Distribution of the classes and subsets of the data sorted by class frequency, each corresponding to $\approx 10\%$ of the samples. **(b)** Overall training loss. **(c, d)** Training loss for each subset for SGD and Adam. **(b)** is the average of **(c, d)**.

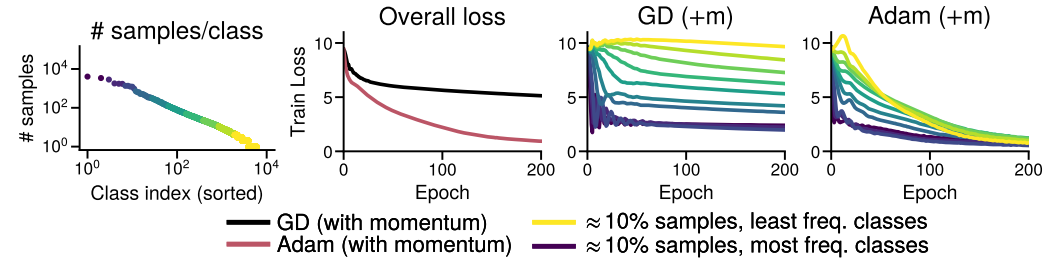

Figure 16: **Similar behavior as Figure 1 on a one-layer transformer with deterministic updates.** Trained on TinyPTB. As in Figure 1, GD makes little to no progress on low-frequency classes while Adam makes progress on all subsets. **(a)** Distribution of the classes and subsets of the data sorted by class frequency, each corresponding to $\approx 10\%$ of the samples. **(b)** Overall training loss. **(c, d)** Training loss for each subset for SGD and Adam. **(b)** is the average of **(c, d)**.

E Comparing normalized GD and sign descent

We compare GD and Adam to normalized GD and sign descent across the problems below. The results show that sign descent leads to similar benefits as Adam on low-frequency classes, and that changing the direction, as in sign descent, has more impact than just changing the magnitude, as in normalized GD.

- Figure 17: Training the last layer of a one-module transformer on TinyPTB.
- Figure 18: A linear model on **Random Heavy-Tailed Labels**, as in Figure 2.
- Figure 19: A one-module transformer on **TinyPTB**, as in Figure 16, training all layers.
- Figure 20: A CNN on **MNIST+Barcoded**, as in Figure 7.

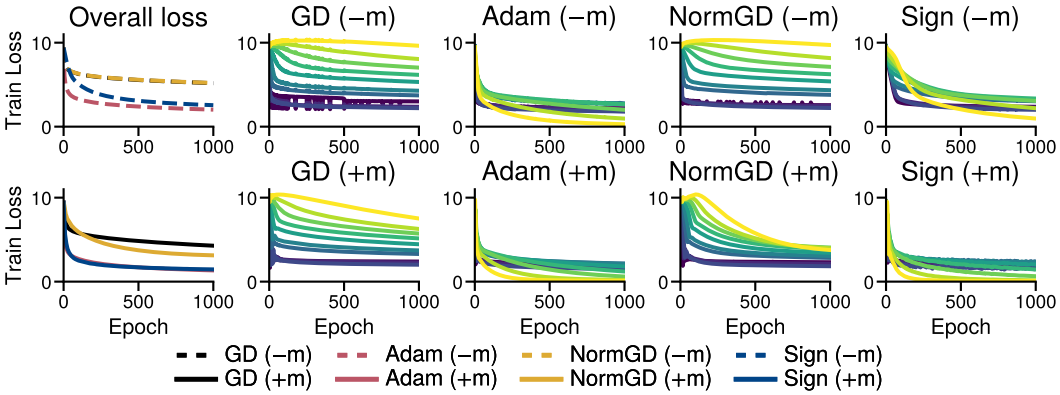

Figure 17: **Sign descent, as a simplified form of Adam, performs well on low-frequency classes.** Training the last layer of a simplified one-layer transformer with GD, Adam, normalized GD, and sign descent, with and without momentum ($\pm$m). Momentum and normalizing the magnitude help but have smaller effects than using sign descent, which recovers similar dynamics to Adam.

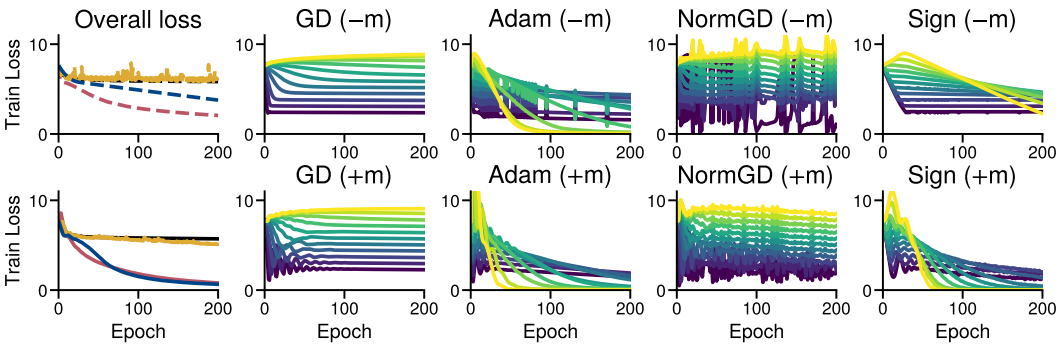

Figure 18: **All optimizers on the linear model of Figure 2.**

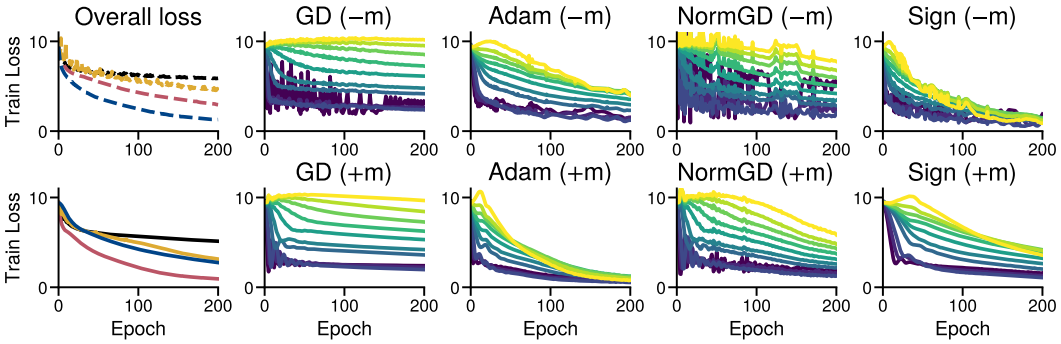

Figure 19: **All optimizers on the transformer of Figure 16.**

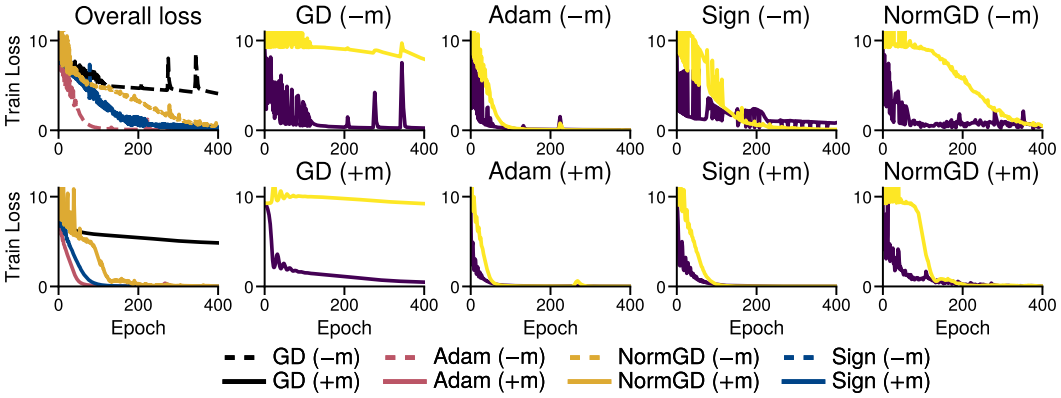

Figure 20: **All optimizers on the CNN of Figure 7.** First column: Overall training loss. Remaining: Loss by frequency groups for each optimizer, with and without momentum (+m, bottom/−m, top).

F Up-weighting low-frequency classes can improve the performance of SGD

To support Section 2.3, we show show that upweighting low-frequency classes helps reduce the performance gap between SGD and Adam on problems with heavy-tailed class imbalance, providing evidence that the optimization difficulties are associated with class imbalance.

While reweighting the loss of samples from class k by $1/\pi_k$ to address the class imbalance seems intuitive, optimizing the reweighted loss is no longer guaranteed to lead to progress on the original loss, especially if the weights are large. Indeed, we find that on some problems this reweighting does not improve performance (although SGD and Adam perform similarly on the reweighted loss, not shown). However, the less extreme reweighting of $1/\sqrt{\pi_k}$ appears to consistently outperform SGD.

In Figure 21, we run SGD on the reweighted loss with the two weighting schemes, $1/\pi_k$ and $1/\sqrt{\pi_k}$ and plot its performance on the original, unweighted loss. We compare the performance of the two reweighting schemes with SGD and Adam, all with momentum, on the following 4 problems.

- The small transformer on PTB in Figure 15 (stochastic training)
- The Linear model on synthetic data in Figure 2 (deterministic training)
- The CNN on the imbalanced MNIST dataset in Figure 7 (deterministic training)
- The ResNet18 on the imbalanced ImageNet dataset in Figure 8 (stochastic training)

We found that the combination of both Adam and reweighting did not improve over running Adam on the original loss and do no include it in Figure 21.

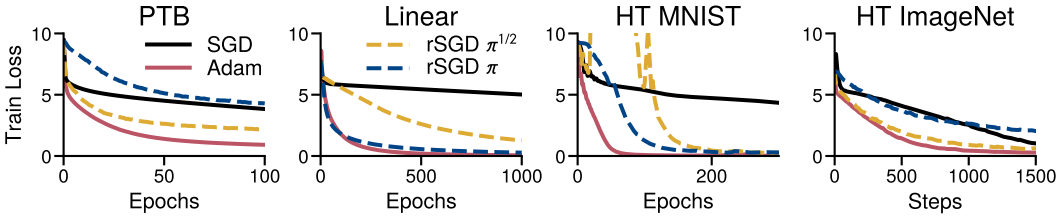

Figure 21: **Reweighting the loss improves the performance of SGD on low-frequency classes.** The plots show the unweighted loss, while SGD and Adam optimize a reweighted loss. Reweighted SGD (rSGD) with weights $1/\sqrt{\pi_k}$ consistently outperforms plain SGD, although it can lead to spikes, as on the CNN on the MNIST dataset. Reweighting with weights $1/\pi_k$ is sometimes better (Linear, MNIST) but can be worse (PTB, ImageNet) as it optimizes a different objective.

G Dynamics of the gradient and Hessian throughout training

This section provides additional details on the dynamics of (S)GD and Adam discussed in Section 3.2.

- Figure 22 shows the dynamics of GD and Adam on the linear model on synthetic data in Figure 2 (deterministic training), and additionally shows the average predicted probabilities p for each frequency group, showing that the deviation from the linear relationship for rare classes coincides with the predicted probabilities p for those classes going to 1.
- The following figures show the correlation on additional problems, on
  - Figure 25 The small transformer on PTB in Figure 15 (stochastic training)
  - Figure 23 The CNN on the imbalanced MNIST dataset in Figure 7 (deterministic training)
  - Figure 24 The ResNet18 on the imbalanced ImageNet dataset in Figure 8 (stochastic training)
- Figure 26 illustrates that this correlation does not hold globally and only emerges throughout training by showing that a *negative* correlation can instead be found by looking at the inverse of the weights, $-\mathbf{W}_t$, over the path taken by Adam.

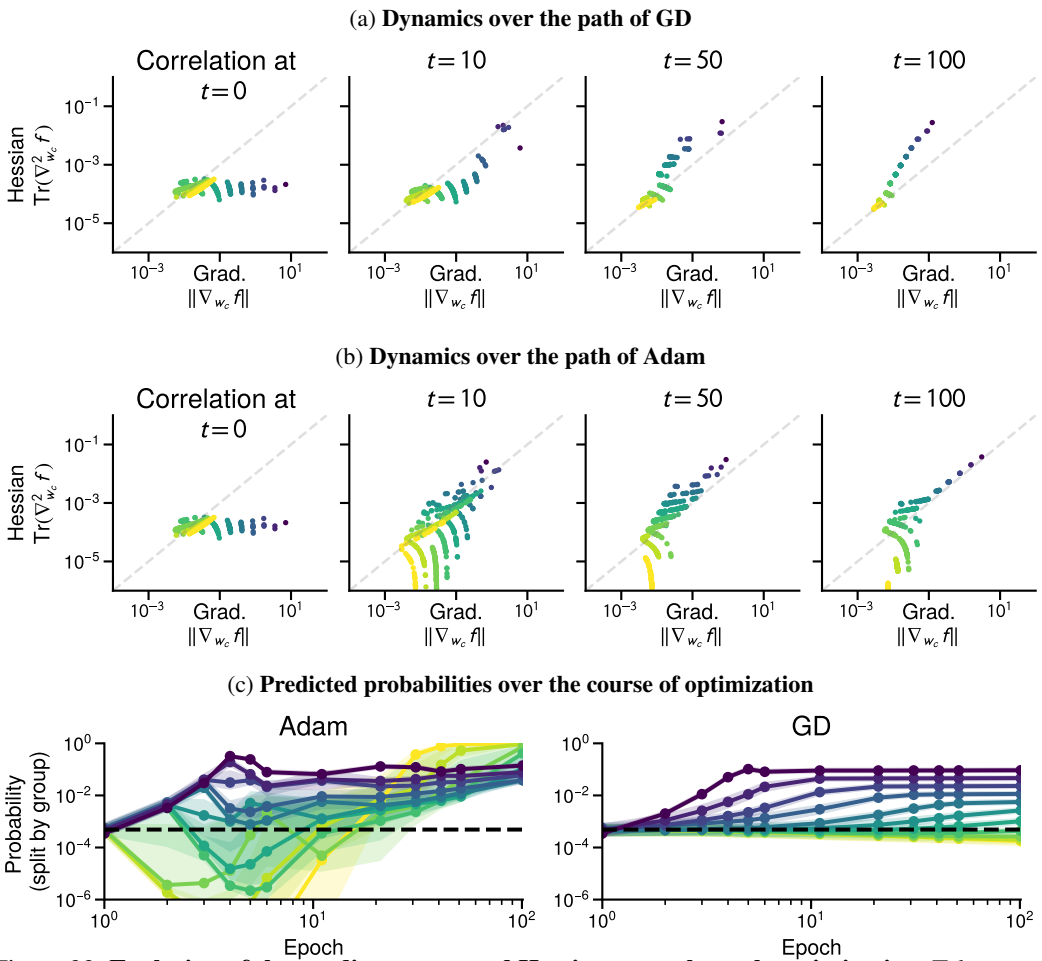

Figure 22: **Evolution of the gradient norm and Hessian trace through optimization.** Taken over the path of GD (a) and Adam (b) on the linear problem of Figure 2. The blocks correspond to the rows $\mathbf{w}_1, ..., \mathbf{w}_c$ of the parameter matrix $\mathbf{W}$. The color indicates the class frequency, showing that lower (higher) frequency classes have smaller (larger) gradient norm and Hessian trace. Figure 22b is a replication of Figure 4, given here for convenience. The deviation from the perfect correlation is explainable by the fact that difference classes are learned at difference speed, leading to a different value of p in Proposition 2, shown in (c). For SGD, frequent classes are learned faster than infrequent ones, while for Adam, p is similar among the most frequent groups of classes while $p \to 1$ for the least frequent classes.

(a) **Dynamics over the path of GD**

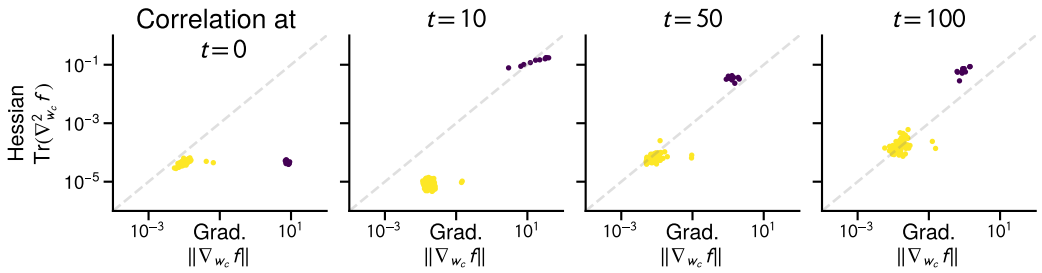

(b) **Dynamics over the path of Adam**

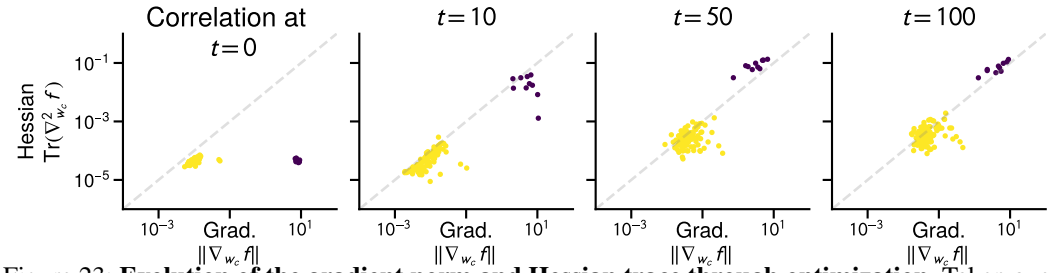

Figure 23: **Evolution of the gradient norm and Hessian trace through optimization.** Taken over the path of GD and Adam on the CNN on imbalanced MNIST in Figure 7. Note that this problem only has two groups of classes with different frequencies; 10 classes have ≈5k samples while 10k classes have 5 samples.

(a) **Dynamics over the path of SGD**

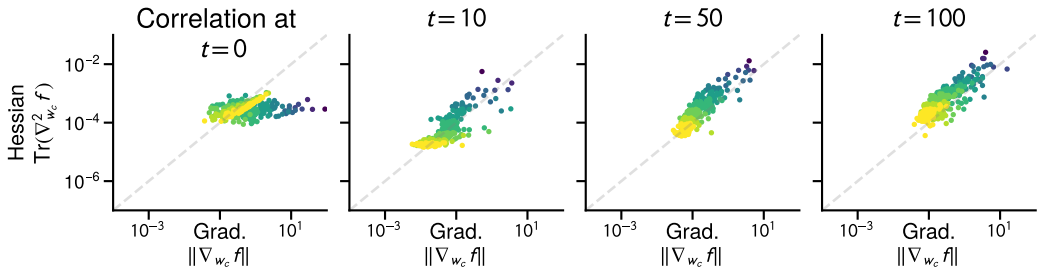

(b) **Dynamics over the path of Adam**

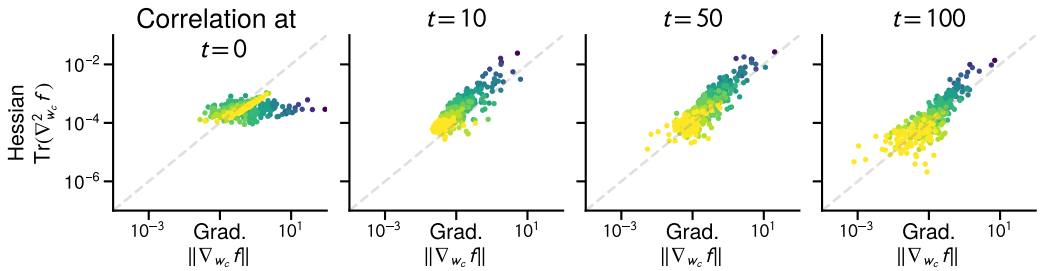

Figure 24: **Evolution of the gradient norm and Hessian trace through optimization.** Taken over the path of SGD and Adam on the ResNet18 on imbalanced ImageNet in Figure 8.

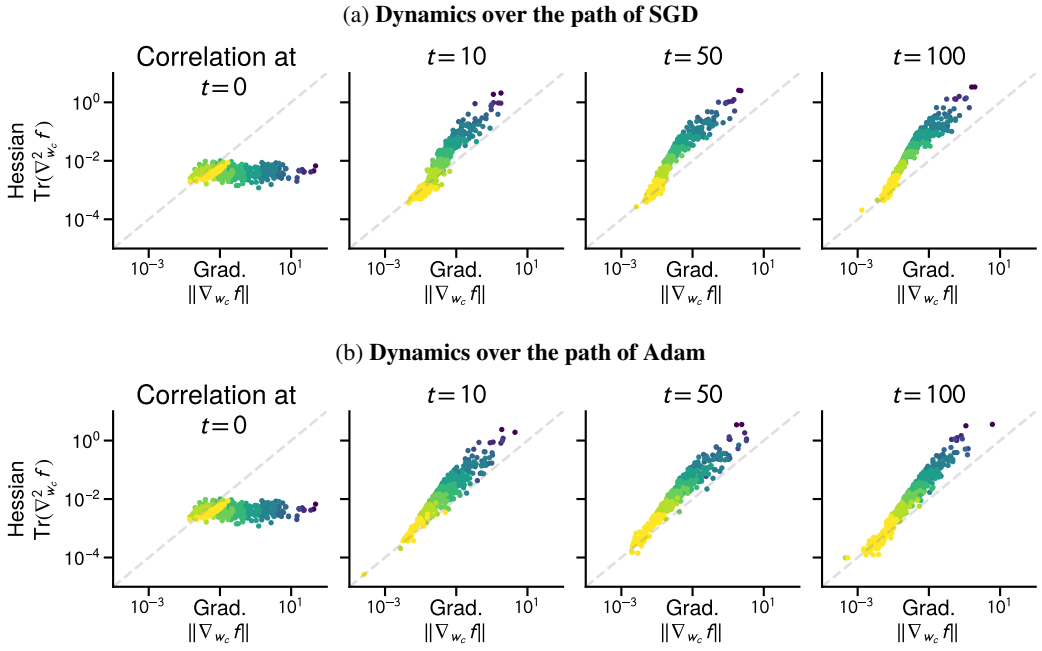

Figure 25: **Evolution of the gradient norm and Hessian trace through optimization.** Taken over the path of SGD and Adam on the small Transformer on PTB in Figure 15.

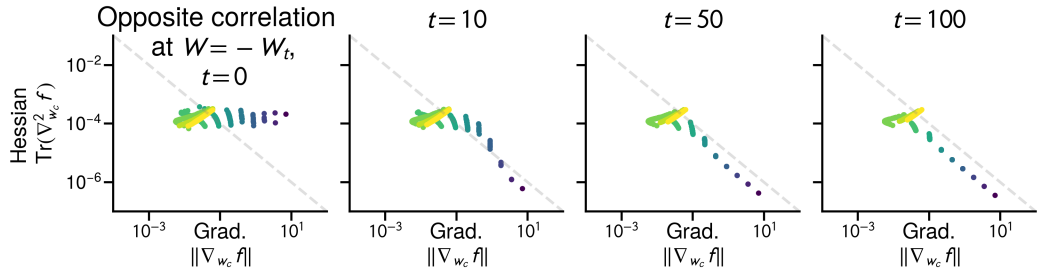

Figure 26: **The correlation only holds while training.** Correlation between the gradient and Hessian blocks through the path $\{-\mathbf{W}_t\}$, where $\mathbf{W}_t$ are the iterates of Adam on the linear model of Figure 2. This illustrates that the correlation described in Proposition 2 is not a global property of the problem and requires that the optimizer make progress and assign samples to their correct classes.

H Correlation between the gradient and Hessian across blocks

This section gives the proof of Proposition 2 in Section 3.2

Proposition 2. *If initialized at $\mathbf{W}_0 = 0$, the gradient and Hessian of the loss $\mathcal{L}$ w.r.t. $\mathbf{w}_k$ are*

$$\nabla_{\mathbf{w}_k} \mathcal{L}(\mathbf{W}_0) = \pi_k \bar{\mathbf{x}}^k - \tfrac{1}{c}\bar{\mathbf{x}}, \qquad \nabla^2_{\mathbf{w}_k} \mathcal{L}(\mathbf{W}_0) = \tfrac{1}{c}\big(1 - \tfrac{1}{c}\big)\bar{\mathbf{H}}, \tag{1}$$

During training, if the model correctly assigns samples to class k with probability p (Assumption 1),

$$\begin{aligned} \nabla_{\mathbf{w}_k} \mathcal{L} &= \ (1-p)\pi_k\, \bar{\mathbf{x}}^k \ + O\big(\tfrac{1}{c}\big), \\ \nabla^2_{\mathbf{w}_k} \mathcal{L} &= p(1-p)\pi_k\, \bar{\mathbf{H}}^k + O\big(\tfrac{1}{c}\big), \end{aligned} \quad \textit{and} \quad \|\nabla_{\mathbf{w}_k} \mathcal{L}\| \sim \left(\frac{1}{p}\frac{\|\bar{\mathbf{x}}^k\|}{\operatorname{Tr}(\bar{\mathbf{H}}^k)}\right) \operatorname{Tr}(\nabla^2_{\mathbf{w}_k} \mathcal{L}) \text{ as } c \to \infty, \tag{2}$$

for classes where the frequency does not vanish too quickly, $\pi_k = \omega(1/c)$.

The requirement that the class frequencies do not vanish, $\pi_k = \omega(1/c)$, is necessary to make it possible to discuss class frequencies as $c \to \infty$, unless the class frequencies do not depend on c. While the frequencies π_k and the number of classes c can be independent, for example if π_k follows an exponential decay, $\pi_k \propto 2^{-k}$, it does not hold for all distributions. While it may seem that this result only holds for relatively frequent classes, as it requires $\pi_k c \to \infty$, we can see that nearly all the data comes from classes where this correlation holds when the classes are distributed as $\pi_k \propto 1/k$. Denote by $H(c) = \sum_{k=1}^{c} 1/k = \Theta(\log c)$. After normalization, we have $\pi_k = 1/kH(c)$. The correlation result holds as long as $\pi_k c \to \infty$, and so it at least holds for the first $k \leq c/\log(c)^2$ classes as $\pi_k c \geq \log(c) \to \infty$. While this only cover a $1/\log(c)^2$ fraction of the classes, those classes account for nearly all the data as

$$\sum_{k=1}^{\lceil \frac{c}{\log(c)} \rceil} \pi_k = \frac{H\big(\lceil c/\log(c)^2 \rceil\big)}{H(c)} = \Theta\left(\frac{\log(c) - 2\log\log(c)}{\log(c)}\right) \to 1.$$

Proof of Proposition 2. We first recall the gradient and Hessian for each block $\mathbf{w}_1, ..., \mathbf{w}_c$;

$$\nabla_{\mathbf{w}_k} \ell(\mathbf{W}, \mathbf{x}, \mathbf{y}) = (\mathbf{1}[y = k] - \mathbf{p}(\mathbf{x})_k)\mathbf{x}, \qquad \nabla^2_{\mathbf{w}_k} \ell(\mathbf{W}, \mathbf{x}, \mathbf{y}) = \mathbf{p}(\mathbf{x})_k(1 - \mathbf{p}(\mathbf{x})_k)\mathbf{x}\mathbf{x}^\top,$$

and the definitions of the moments of the data, per class and overall.

$$\bar{\mathbf{x}}^k = \tfrac{1}{n_k}\textstyle\sum_{i=1:y_i=k}^{n} \mathbf{x}_i, \quad \bar{\mathbf{x}} = \tfrac{1}{n}\textstyle\sum_{i=1}^{n} \mathbf{x}_i, \quad \bar{\mathbf{H}}^k = \tfrac{1}{n_k}\textstyle\sum_{i=1:y_i=k}^{n} \mathbf{x}_i\mathbf{x}_i^\top, \quad \bar{\mathbf{H}} = \tfrac{1}{n}\textstyle\sum_{i=1}^{n} \mathbf{x}_i\mathbf{x}_i^\top.$$

Our first step is to rewrite the sums for the gradient and Hessian to separate the influence of the samples of the correct class k and the other samples.

$$\begin{aligned} \nabla_{\mathbf{w}_k} \mathcal{L}(\mathbf{W}) &= \frac{1}{n}\sum_{i=1}^{n} (\mathbf{1}[y_i = k] - \mathbf{p}(\mathbf{x}_i)_k)\mathbf{x}_i, \\ &= \frac{1}{n}\sum_{j=1}^{c}\sum_{i:y_i=j} (\mathbf{1}[y_i = k] - \mathbf{p}(\mathbf{x}_i)_k)\mathbf{x}_i, && \text{(Split by class)} \\ &= \sum_{j=1}^{c}\frac{\pi_j}{n_j}\sum_{i:y_i=j} (\mathbf{1}[y_i = k] - \mathbf{p}(\mathbf{x}_i)_k)\mathbf{x}_i, && \text{(Use class frequencies } \pi_j = n_j/n) \\ &= \pi_k \frac{1}{n_k}\sum_{i=1:y_i=k}^{n} (1 - \mathbf{p}(\mathbf{x}_i)_k)\mathbf{x}_i + \sum_{j=1, j\neq k}^{c}\frac{\pi_j}{n_j}\sum_{i:y_i=j} (-\mathbf{p}(\mathbf{x}_i)_k)\mathbf{x}_i. \\ \nabla^2_{\mathbf{w}_k} \mathcal{L}(\mathbf{W}) &= \frac{1}{n}\sum_{i=1}^{n} \mathbf{p}(\mathbf{x}_i)_k(1 - \mathbf{p}(\mathbf{x}_i)_k)\mathbf{x}_i\mathbf{x}_i^\top, \\ &= \frac{\pi_k}{n_k}\sum_{i:y_i=k} \mathbf{p}(\mathbf{x}_i)_k(1 - \mathbf{p}(\mathbf{x}_i)_k)\mathbf{x}_i\mathbf{x}_i^\top + \sum_{j=1, j\neq k}^{c}\frac{\pi_j}{n_j}\sum_{i:y_i=j} \mathbf{p}(\mathbf{x}_i)_k(1 - \mathbf{p}(\mathbf{x}_i)_k)\mathbf{x}_i\mathbf{x}_i^\top. \end{aligned}$$

We can simplify the first terms using the assumption that $p(\mathbf{x}_i)_k = p$ for samples of the correct class,

$$\frac{\pi_k}{n_k}\sum_{i=1:y_i=k}^{n} (1 - \mathbf{p}(\mathbf{x}_i)_k)\mathbf{x}_i = (1-p)\pi_k\bar{\mathbf{x}}^k, \quad \frac{\pi_k}{n_k}\sum_{i:y_i=k} \mathbf{p}(\mathbf{x}_i)_k(1 - \mathbf{p}(\mathbf{x}_i)_k)\mathbf{x}_i\mathbf{x}_i^\top = p(1-p)\pi_k\bar{\mathbf{H}}^k.$$

We introduce the following shorthands for the second terms,

$$\mathbf{d}_k = c \sum_{j=1, j\neq k}^{c} \frac{\pi_j}{n_j} \sum_{i:y_i=j} (-\mathbf{p}(\mathbf{x}_i)_k)\mathbf{x}_i, \qquad \mathbf{D}_k = c \sum_{j\neq k} \frac{\pi_j}{n_j} \sum_{i:y_i=j} \mathbf{p}(\mathbf{x}_i)_k(1-\mathbf{p}(\mathbf{x}_i)_k)\mathbf{x}_i\mathbf{x}_i^\top.$$

Using those simplifications, we obtain that

$$\nabla_{\mathbf{w}_k}\mathcal{L}(\mathbf{W}) = (1-p)\pi_k\bar{\mathbf{x}}^k + \frac{1}{c}\mathbf{d}_k, \qquad \nabla^2_{\mathbf{w}_k}\mathcal{L}(\mathbf{W}) = p(1-p)\pi_k\bar{\mathbf{H}}^k + \frac{1}{c}\mathbf{D}_k.$$

The terms $\mathbf{d}_k$, $\mathbf{D}_k$ are averages of terms weighted by $c\mathbf{p}(\mathbf{x}_i)_k$, which by assumption is $O(1)$, and as such both $\|\mathbf{d}_k\|$ and $\mathrm{Tr}(\mathbf{D}_k)$ are $O(1)$. The ratio between the two will be dominated by the contribution of their first term as long as π_k dominates $1/c$, in the sense that $\lim_{c\to\infty} \frac{1}{\pi_k c} \to 0$, as

$$\lim_{c\to\infty} \frac{\|\nabla_{\mathbf{w}_k}\mathcal{L}\|}{\mathrm{Tr}(\nabla^2_{\mathbf{w}_k}\mathcal{L})} = \lim_{c\to\infty} \frac{\left\|(1-p)\bar{\mathbf{x}}^k + \frac{1}{c\pi_k}\mathbf{d}_k\right\|}{\mathrm{Tr}(p(1-p)\pi_k\bar{\mathbf{H}}^k + \frac{1}{c\pi_k}\mathbf{D}_k)} = \frac{1}{p}\frac{\|\bar{\mathbf{x}}^k\|}{\mathrm{Tr}(\bar{\mathbf{H}}^k)}. \qquad \square$$

H.1 Off-diagonal blocks are orders of magnitude smaller than diagonal blocks

Our discussion Section 3.2 ignored the impact of off-diagonal blocks. In this section, we show that they are small. The diagonal and off-diagonal blocks of the matrix for $k \neq k'$.

$$\begin{aligned} & & \mathbf{H}_{kk} &:= \nabla^2_{\mathbf{w}_k}\ell(\mathbf{W},\mathbf{x},y) &&= \mathbf{p}(\mathbf{x})_k(1-\mathbf{p}(\mathbf{x})_k)\mathbf{x}\mathbf{x}^\top, \\ \text{and for } j\neq k, & & \mathbf{H}_{kj} &:= \nabla_{\mathbf{w}_k}\nabla_{\mathbf{w}_{k'}}\ell(\mathbf{W},\mathbf{x},\mathbf{y}) &&= \mathbf{p}(\mathbf{x})_k(\ \ -\mathbf{p}(\mathbf{x})_{k'})\mathbf{x}\mathbf{x}^\top. \end{aligned}$$

From this, we can see that, on average, the magnitude of the off-diagonal blocks will be smaller than that of the diagonal blocks, as

$$\mathbf{H}_{kk} = -\textstyle\sum_{j=1,j\neq k}^{c} \mathbf{H}_{kj},$$

because $\sum_{k'=1,k'\neq k}^{c} \mathbf{p}(\mathbf{x})_k\mathbf{p}(\mathbf{x})_{k'} = \mathbf{p}(\mathbf{x})_k(1-\mathbf{p}(\mathbf{x})_k)$, This means that the matrix $\mathbf{T} : [c\times c]$ formed by taking the trace of the blocks, $\mathbf{T}_{jk} = \mathrm{Tr}(\mathbf{H}_{jk})$, is diagonally dominant.

Figure 27 show that the magnitude of the entries of the Hessian in off-diagonal blocks is orders of magnitude smaller than those of the diagonal blocks. Instead of plotting the $[cd\times cd]$ Hessian, we subsample 40 classes and 40 input dimensions and plot the resulting $[160\times 160]$ entries at different points throughout the trajectory of Adam on the problem of Figure 2. Figure 27 shows the matrices with classes sampled uniformly and Figure 27 with classes sampled log-uniformly

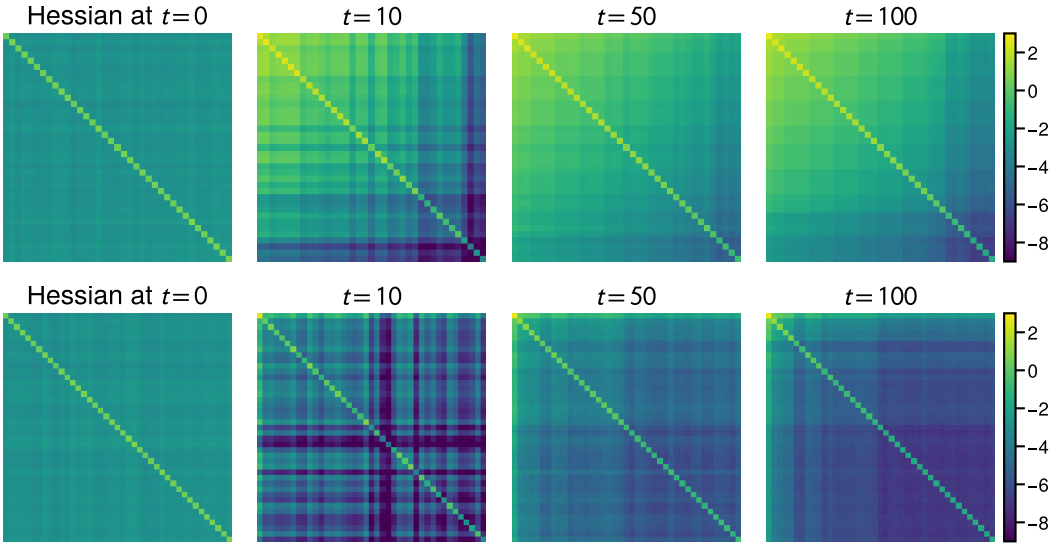

Figure 27: **The diagonal Hessian blocks are orders of magnitude larger than off-diagonal blocks.** Showing the magnitude of a subset of the Hessian blocks ($\log_{10}(|\mathrm{Tr}(\nabla^2_{ij}\mathcal{L})|)$) for a $[160\times 160]$ subset of the Hessian. **Top:** sampling 40 classes log-uniformly and 40 input dimensions uniformly. **Bottom:** sampling 40 classes and 40 input dimensions uniformly.

I Continuous time GD and sign descent on a simple imbalanced problem

We give the proof of Theorem 3 on the simple imbalanced setting, restated here for convenience.

Simple imbalanced setting. *Consider c classes with frequencies $\pi_1, ..., \pi_c$ where all samples from a class are the same, $\mathbf{x}_i = \mathbf{e}_k$ if $y_i = k$, where $\mathbf{e}_k$ is the kth standard basis vector in $\mathbb{R}^c$.*

Theorem 3. *On the* simple imbalanced setting*, gradient flow and continuous time sign descent initialized at $\mathbf{W} = 0$ minimize the loss of class k, $\ell_k(t) = -\log(\sigma(\mathbf{W}(t)\mathbf{e}_k)_k)$, at the rate*

$$\textit{Gradient flow:} \quad \ell_k(t) = \Theta(1/\pi_k t), \qquad \textit{Continuous time sign descent:} \quad \ell_k(t) = \Theta\left(e^{-ct}\right).$$

We separate the proof for gradient flow into 3 parts. Lemma 4 simplifies the dynamics into smaller, independent differential equations, Lemma 5 solves the differential equation and Lemma 6 bounds the loss. We treat continuous time sign descent separately in Lemma 7.

Notation. If $\mathbf{W}$ is a $[a \times b]$ matrix, then $\mathbf{w}_1, ..., \mathbf{w}_a$ are the rows and $\mathbf{w}^1, ..., \mathbf{w}^b$ are the vectors, and w_{ij} is the entry at the ith column, jth row. For brevity, we use $z = c - 1$ as the term appears often.

Lemma 4 (Separation of the dynamics)**.** *The dynamics of the parameter matrix $\mathbf{W}$ separate into c 2-dimensional differential equations, $w_{kk}(t) = a_k(t)$ and $w_{jk}(t) = b_k(t)$ for $j \neq k$, where*

$$\begin{aligned} a_k(0) &= 0, & \frac{\mathrm{d}}{\mathrm{d}t} a_k &= \pi_k \left(1 - \frac{\exp(a_k)}{\exp(a_k) + (c-1)\exp(b_k)}\right), \\ b_k(0) &= 0, & \frac{\mathrm{d}}{\mathrm{d}t} b_k &= \pi_k \left(\quad - \frac{\exp(b_k)}{\exp(a_k) + (c-1)\exp(b_k)}\right). \end{aligned}$$

Proof. Our goal is to simplify the dynamics starting at $\mathbf{W}(0) = 0$ and following the gradient flow $\frac{\mathrm{d}}{\mathrm{d}t}\mathbf{W} = -\nabla\mathcal{L}(\mathbf{W})$, where $\mathbf{W} : [c \times d]$. For the simplified setting, we have that $d = c$ are the inputs are the standard basis vectors in $\mathbb{R}^c$. The derivative of $\mathcal{L}$ w.r.t. a single element w_{kj} is

$$\partial_{w_{kj}} \mathcal{L}(\mathbf{W}) = -\pi_k \mathbf{1}[k = j] + \pi_j \sigma(\mathbf{w}^j)_k.$$

As $\partial_{w_{kj}}$ only depends on $\mathbf{w}^j$ for all k, The dynamics are independent across the columns of $\mathbf{W}$, giving c independent equations in $\mathbb{R}^c$,

$$\mathbf{w}^j(0) = 0, \qquad \frac{\mathrm{d}}{\mathrm{d}t}\mathbf{w}^j = \pi_j(\mathbf{e}_j - \sigma(\mathbf{w}^j)).$$

To further simplify the dynamics, we use the fact that the weights that are not associated with the correct class have the same dynamics. For any indices i, j different from k, $w_{ik}(t) = w_{jk}(t)$. They have the same derivatives if they have the same value, as

$$-\frac{\mathrm{d}}{\mathrm{d}t} w_{ik} = \pi_k \sigma(\mathbf{w}^k)_i = \pi_k \frac{\exp(w_{ik})}{\sum_{k'} \exp(w_{k'k})} = \pi_k \frac{\exp(w_{jk})}{\sum_{k'} \exp(w_{k'k})} = \pi_k \sigma(\mathbf{w}^k)_j = -\frac{\mathrm{d}}{\mathrm{d}t} w_{jk},$$

so they will have the same dynamics and the equation can be reduced to a system of 2 variables, $w_{kk} = a_k$ and $w_{jk} = b_k$ for any $j \neq k$, with

$$\begin{aligned} a_k(0) &= 0, & \frac{\mathrm{d}}{\mathrm{d}t} a_k &= \pi_k \left(1 - \frac{\exp(a_k)}{\exp(a_k) + (c-1)\exp(b_k)}\right), \\ b_k(0) &= 0, & \frac{\mathrm{d}}{\mathrm{d}t} b_k &= \pi_k \left(\quad - \frac{\exp(b_k)}{\exp(a_k) + (c-1)\exp(b_k)}\right). \end{aligned}$$

□

Lemma 5 (Solution of the dynamics)**.** *For a given class with frequency π, the dynamics of the parameters a and b in Lemma 4 evolve as follows, using the shortcuts $f(t) = 1 + c\pi t$ and $z = c - 1$,*

$$a(t) = \frac{1}{c}\left(f(t) - zW\left(\frac{1}{z}\exp\left(\frac{1}{z}f(t)\right)\right)\right) \qquad b(t) = -\frac{1}{z}a(t),$$

Proof. We want the solution to the differential equation

$$a(0) = 0 \qquad \frac{\mathrm{d}}{\mathrm{d}t}a = \pi\left(1 - \frac{\exp(a)}{\exp(a) + (c-1)\exp(b)}\right),$$
$$b(0) = 0 \qquad \frac{\mathrm{d}}{\mathrm{d}t}b = \pi\left(- \frac{\exp(b)}{\exp(a) + (c-1)\exp(b)}\right).$$

The general solution, ignoring the initial conditions, uses the Lambert W function and constants K_1, K_2.[1] For brevity, we introduce the shortcut $z = c - 1$.

$$a(t) = \frac{1}{zc}\left(ce^{-K_1}K_2 + cz\pi t - z^2 W\left(\frac{1}{z}\exp\left(\frac{c}{z^2}\left(z\pi t + e^{-K_1}K_2\right) - K_1\right)\right)\right),$$
$$b(t) = K_1 - \frac{1}{z^2 c}\left(ce^{-K_1}K_2 + cz\pi t - z^2 W\left(\frac{1}{z}\exp\left(\frac{c}{z^2}\left(z\pi t + e^{-K_1}K_2\right) - K_1\right)\right)\right).$$

We need to set K_1, K_2 to satisfy the initial conditions $a(0) = b(0) = 0$. As $b(t) = K_1 - a(t)/z$, we must have that $K_1 = 0$, giving the simplification

$$a(t) = \frac{1}{zc}\left(cK_2 + cz\pi t - z^2 W\left(\frac{1}{z}\exp\left(\frac{c}{z^2}(z\pi t + K_2) - K_1\right)\right)\right), \qquad b(t) = -\frac{1}{z}a(t).$$

To set K_2, we need to have

$$0 = zca(0) = cK_2 - z^2 W\left(\frac{1}{z}\exp\left(K_2\frac{c}{z^2}\right)\right) \implies W\left(\frac{1}{z}\exp\left(K_2\frac{c}{z^2})\right)\right) = \frac{c}{z^2}K_2$$

Since $W(xe^x) = x$ for $x > 0$, the equation is satisfied for $K_2 = \frac{z}{c}$, as we get $W\left(\frac{1}{z}e^{\frac{1}{z}}\right) = \frac{1}{z}$, giving

$$a(t) = \frac{1}{c}\left(1 + c\pi t - zW\left(\frac{1}{z}\exp\left(\frac{1}{z}(1 + c\pi t)\right)\right)\right) \qquad b(t) = -\frac{1}{z}a(t). \qquad \square$$

Lemma 6 (Bound for the loss)**.** *For t sufficiently large such that $1 + c\pi_k t \geq z\log z + 1$,*

$$\ell_k(t) = \Theta\left(\frac{1}{\pi_k t}\right).$$

Using the simplification derived in Lemma 4 and the solution of the differential equation in Lemma 5, we can rewrite the loss for a specific class as a function of time as

$$L_k(\mathbf{W}) \coloneqq -\log(\sigma(\mathbf{W}\mathbf{e}_k)_k) = -\log\left(\frac{\exp(w_{kk})}{\sum_{j=1}^{c}\exp(w_{jk})}\right),$$
$$\ell_k(t) \coloneqq L_k(\mathbf{W}(t)) = -\log\left(\frac{\exp(a_k(t))}{\exp(a_k(t)) + (c-1)\exp(b_k(t))}\right) = \log(1 + (c-1)\exp(cb_k(t))),$$

where the equality uses that $a_k(t) = (c-1)b_k(t)$. For brevity, we will drop the index k in a_k, b_k, ℓ_k and π_k and use the shortcut $z = c - 1$, bounding the quantity

$$\ell(t) = \log(1 + z\exp(cb(t))).$$

Expanding the definition of $b(t)$ using Lemma 5, we have

$$z\exp(cb(t)) = z\exp\left(-\frac{1}{z}\left(f(t) - zW\left(\frac{1}{z}\exp\left(\frac{1}{z}f(t)\right)\right)\right)\right), \quad \text{where} \quad f(t) = 1 + c\pi t.$$

To simplify the W function, we use the fact that for $x > e$ (Hoorfar and Hassani, 2008, Theorem 2.7)

$$W(x) = \log(x) - \log(\log(x)) + \delta(x) \qquad \text{where} \qquad \frac{1}{2} \leq \delta(x)\frac{\log(x)}{\log(\log(x))} \leq \frac{e}{e-1}.$$

[1] WolframAlpha solution for $\pi = 1$: https://www.wolframalpha.com/input?i=d/dt+x(t)+=+1-exp(x(t))/(exp(x(t))+c*exp(y(t))),+d/dt+y(t)+=+-exp(y(t))/(exp(x(t))+c*exp(y(t)))

To use this bound on $W\big(\frac{1}{z}\exp\big(\frac{1}{z}f(t)\big)\big)$, we need $\frac{1}{z}\exp\big(\frac{1}{z}f(t)\big) \geq e$, which is satisfied for t sufficiently large, once $f(t) \geq z(\log z + 1)$.

Using that $\log\big(\frac{1}{z}\exp\big(\frac{1}{z}f(t)\big)\big) = \frac{1}{z}f(t) - \log(z)$, and writing $h(t) = \delta\big(\frac{1}{z}\exp\big(\frac{1}{z}f(t)\big)\big)$, we have

$$\begin{aligned} f(t) - zW\left(\frac{1}{z}\exp\left(\frac{1}{z}f(t)\right)\right) &= f(t) - z\left(\frac{1}{z}f(t) - \log(z) - \log\left(\frac{1}{z}f(t) - \log(z)\right) + h(t)\right), \\ &= z(\log(f(t) - z\log(z)) - h(t)), \end{aligned}$$

giving the simplification

$$\begin{aligned} z\exp(cb(t)) &= z\exp\left(-\frac{1}{z}\left(f(t) - zW\left(\frac{1}{z}\exp\left(\frac{1}{z}f(t)\right)\right)\right)\right), \\ &= z\exp(-\log(f(t) - z\log(z)) + h(t)) = \frac{z\exp(h(t))}{f(t) - z\log z}, \end{aligned}$$

This gives the average loss

$$\ell(t) = \log(1 + z\exp(cb(t))) = \log\left(1 + \frac{z\exp(h(t))}{f(t) - z\log z}\right)$$

To bound this expression, we can use that $\frac{z\exp(h(t))}{f(t) - z\log z} \geq 0$ after $f(t) \geq z\log z$, which we have already assumed to apply the bound on the W function, and use the bounds $\frac{x}{1+x} \leq \log(1+x) \leq x$ to get

$$\frac{z\exp(h(t))}{f(t) - z\log z + z\exp(h(t))} \leq \ell(t) \leq \frac{z\exp(h(t))}{f(t) - z\log z}.$$

As $h(t)$ is upper bounded by a constant and $\lim_{t\to\infty} h(t) = 0$, $\lim_{t\to\infty}\exp(h(t)) = 1$, we have

$$\ell(t) = \Theta\left(\frac{z}{f(t) - z\log z}\right) = \Theta\left(\frac{1}{\pi t}\right).$$

Lemma 7. *The loss at time t for continuous time sign descent is $\ell_k(t) = \log(1 + (c-1)\exp(-ct))$*

Proof. The same decomposition as in Lemma 4 hold, with the dynamics

$$a_k(0) = 0, \qquad \frac{\mathrm{d}}{\mathrm{d}t}a_k = 1, \qquad a_k(t) = t, \qquad\qquad b_k(0) = 0, \qquad \frac{\mathrm{d}}{\mathrm{d}t}b_k = -1, \qquad b_k(t) = -t,$$

leading to the following loss

$$\ell_k(t) = \log(1 + (c-1)\exp(-ct)) = \Theta(z\exp(-ct)).$$ □

J Discussion and limitations

Interaction with stochasticity. Our experiments include both stochastic and deterministic training regimes and show that stochasticity is not the cause of the slow performance of SGD on low-frequency classes, as it already appears between full batch GD and Adam. This observation is consistent with prior work showing that the performance gap between SGD and Adam on language transformers already appears with deterministic training (Kunstner et al., 2023). However, we do not attempt to quantify the interaction between stochasticity and class imbalance and leave it for future work.

Training performance vs. generalization. Our main focus is on optimization performance. Our observations need not generalize to the validation loss, especially in settings prone to overfitting, as good training performance may lead to overfitting on classes with few samples (Sagawa et al., 2020) However, some form of memorization might be needed in long-tailed settings (Feldman, 2020), and if SGD cannot even fit the training data, generalization cannot be good. On the transformer of Figure 1, we observe similar dynamics across frequencies on the validation loss, shown Appendix A.8. Training dynamics on the empirical and population loss are also often similar, particularly early in training (see, e.g., Nakkiran et al., 2021; Ghosh et al., 2022), and the one-pass training regime commonly used in large language models might mitigate those issues by blurring the line between train and test loss.

Additional difficulties due to text data. We study the effect of the distribution of the classes, the *next* token to be predicted, but other optimization difficulties might arise from the heavy-tailedness of text data. For example, the sequence of tokens used as inputs to the embedding layer are also heavy-tailed. This imbalance might lead to slow progress on embeddings for rare tokens with GD, giving another potential cause for a performance gap. Full sentences (Williams et al., 2015) and latent rules or mechanisms required to understand a paragraph (Michaud et al., 2023) may also display heavy tails, and Adam could be beneficial if those are captured by intermediate layers (e.g., Meng et al., 2022; Wang et al., 2023; Bietti et al., 2023). The choice of tokenization has also been shown to impact downstream performance, which has been attributed to the lack of samples on rare tokens (Gowda and May, 2020) and the improved efficiency of more uniform tokenizers (Zouhar et al., 2023). Our results indicate that tokenization also has a large impact on optimization performance.

Difficulties due to architectures. Beyond the class distribution, additional optimization difficulties may arise from the architectures, due to depth, signal propagation (Noci et al., 2022; He et al., 2023), vanishing gradients and higher order derivatives (Liu et al., 2020; Orvieto et al., 2022). The simplified transformer of Ahn et al. (2023) also exhibits many of the difficulties observed in the literature on regression instead of a classification problem. However, a phenomenon similar to the assignment mechanism could still explain the benefit of Adam. The oscillations in the loss observed at the feature level by Rosenfeld and Risteski (2023) suggests a link between subsets of the samples and subsets of the parameters. For example, if a convolution filter detects a specific background color and captures a specific feature of the data, the magnitude of the gradient and Hessian at intermediate layers could be influenced by the relative frequency of the feature in the data, leading to another form of imbalance.